Monthly Notices
of the
ROYAL ASTRONOMICAL SOCIETY

Mon. Not. R. Astron. Soc. **403,** 1592–1610 (2010) doi:10.1111/j.1365-2966.2009.16223.x

Bolometric correction and spectral energy distribution of cool stars in Galactic clusters⋆

A. Buzzoni,[1]† L. Patelli,[1] M. Bellazzini,[1] F. Fusi Pecci[1] and E. Oliva[2]

[1]*INAF - Osservatorio Astronomico di Bologna, Via Ranzani 1, 40127 Bologna, Italy*
[2]*INAF - Osservatorio Astrofisico di Arcetri, L.go E. Fermi 5, 50125 Firenze, Italy*

Accepted 2009 December 16. Received 2009 December 11; in original form 2009 September 16

Downloaded from https://academic.oup.com/mnras/article/403/3/1592/1050826 by INAF –IASF Bologna user on 17 January 2023

ABSTRACT

We have investigated the relevant trend of the bolometric correction (BC) at the cool-temperature regime of red giant stars and its possible dependence on stellar metallicity. Our analysis relies on a wide sample of optical–infrared spectroscopic observations, along the 3500 Å ⇒ 2.5 μm wavelength range, for a grid of 92 red giant stars in five (three globular + two open) Galactic clusters, along the full metallicity range covered by the bulk of the stars, $-2.2 \leq$ [Fe/H] $\leq +0.4$.

Synthetic $BVR_{\rm C}I_{\rm C}JHK$ photometry from the derived spectral energy distributions allowed us to obtain robust temperature ($T_{\rm eff}$) estimates for each star, within ±100 K or less. According to the appropriate temperature estimate, blackbody extrapolation of the observed spectral energy distribution allowed us to assess the unsampled flux beyond the wavelength limits of our survey. For the bulk of our red giants, this fraction amounted to 15 per cent of the total bolometric luminosity, a figure that raises up to 30 per cent for the coolest targets ($T_{\rm eff} \lesssim$ 3500 K). Overall, we obtain stellar $M_{\rm bol}$ values with an internal accuracy of a few percentages. Even neglecting any correction for lost luminosity etc., we would be overestimating $M_{\rm bol}$ by $\lesssim$0.3 mag, in the worst cases. Making use of our new data base, we provide a set of fitting functions for the V and K BC versus $T_{\rm eff}$ and versus $(B-V)$ and $(V-K)$ broad-band colours, valid over the interval $3300 \leq T_{\rm eff} \leq 5000$ K, especially suited for red giants.

The analysis of the $\rm BC_V$ and $\rm BC_K$ estimates along the wide range of metallicity spanned by our stellar sample shows no evident drift with [Fe/H]. Things may be different for the B-band correction, where the blanketing effects are more and more severe. A drift of $\Delta(B-V)$ versus [Fe/H] is in fact clearly evident from our data, with metal-poor stars displaying a 'bluer' $(B-V)$ with respect to the metal-rich sample, for fixed $T_{\rm eff}$.

Our empirical bolometric corrections are in good overall agreement with most of the existing theoretical and observational determinations, supporting the conclusion that (a) $\rm BC_K$ from the most recent studies are reliable within $\lesssim$±0.1 over the whole colour/temperature range considered in this paper, and (b) the same conclusion apply to $\rm BC_V$ only for stars warmer than ≃3800 K. At cooler temperatures the agreement is less general, and MARCS models are the only ones providing a satisfactory match to observations, in particular in the $\rm BC_V$ versus $(B-V)$ plane.

Key words: stars: atmospheres – stars: late-type – globular clusters: general – Galaxy: stellar content – infrared: stars.

1 INTRODUCTION

A physical assessment of the bolometric emission of stars is a mandatory step for any attempt to self-consistently link observations and theoretical predictions of stellar evolution. The importance of this comparison actually reverberates into a wide range of primary astrophysical questions, ranging from the validation of the reference input physics for nuclear reactions in the stellar interiors to the study of integrated spectrophotometric properties of distant galaxies, through stellar population synthesis models.

By definition, the effective temperature ($T_{\rm eff}$) and physical size (R) of a star provide the natural constraint to its emerging flux, as $L \propto R^2 T_{\rm eff}^4$. If L is a known property for a star, then we could physically

⋆Based on observations made at La Palma, at the Spanish Observatorio del Roque de los Muchachos of the IAC, with the Italian Telescopio Nazionale Galileo (TNG) operated by the Fundación Galileo Galilei of INAF.

†E-mail: alberto.buzzoni@oabo.inaf.it

© 2010 The Authors. Journal compilation © 2010 RAS

'rescale' the spectral energy distribution (SED), and infer, from the observed flux, the distance of the body, d, or its absolute size (R), through a measure of the apparent angular extension, $\theta = (R/d)^2 \propto L\,T_{\rm eff}^{-4}\,d^{-2}$ (Ridgway et al. 1980; Dyck et al. 1996; Perrin et al. 1998; Richichi et al. 1998).

As is well known, however, L cannot, in principle, be measured *directly*, a task for which an ideal detector that is equally sensitive to the whole spectral range is required. The lack of this crucial piece of information is often palliated by indirect observing methods, trying to pick up the bulk of stellar emission through broad-band photometry within the appropriate spectral range according to target temperature.[1] Relying on this approach, Johnson (1966) derived the bolometric versus temperature scale for red giant stars, while Code et al. (1976) explored the same relation for hot early-type stars, through satellite-borne ultraviolet (UV) observations. As an alternative way, many authors tried a fully theoretical assessment of the problem, by studying the $f_{\rm bol}$ versus f_λ relationship on the basis of model grids of stellar atmospheres and thus replacing observations with synthetic photometry directly computed on the theoretical SED (Bessell, Castelli & Plez 1998; Bertone et al. 2004).

Rather than focussing on luminosity, Wesselink (1969) originally proposed a further application of this method, just looking at the bolometric surface brightness, namely $\mu = f_{\rm bol}/\theta^2$, to lead to a refined temperature scale of stars in force of the fundamental relationship $\mu = \sigma\,T_{\rm eff}^{-4}$ (σ being the Stefan–Boltzmann constant). The so-called surface-brightness technique, then better recognized as the IR-flux method (IRFM), has been applied extensively to the study of red giant and supergiant stars (Blackwell, Shallis & Selby 1979; di Benedetto & Rabbia 1987; Blackwell & Lynas-Gray 1994; Alonso, Arribas & Martínez-Roger 1999; Ramírez & Meléndez 2005; González Hernández & Bonifacio 2009), taking advantage of its distance-independent results, providing to match the angular measure of stellar radii with the estimate of the bolometric flux from infrared observations, i.e. $\mu = (f_{\rm bol}/f_{\rm IR})\,f_{\rm IR}$.

Although in different forms, all the previous methods used theoretical models of stellar atmospheres to derive the appropriate 'correcting factor' $\mathcal{R} = f_{\rm bol}/f(\lambda)$ and convert observed or synthetic monochromatic magnitudes $m(\lambda)$ to the bolometric scale.[2]

Taking the Sun as a reference source for our calibration, we could write more explicitly:

$$[m_{\rm bol} - m(\lambda)] - [m_{\rm bol} - m(\lambda)]_\odot = -2.5\,\log(\mathcal{R}/\mathcal{R}_\odot). \quad (1)$$

Equation (1) actually leads to the straight definition of bolometric correction, BC(λ), namely

$${\rm BC}(\lambda) = [m_{\rm bol} - m(\lambda)] = -2.5\,\log\mathcal{R} + {\rm BC}(\lambda)_\odot. \quad (2)$$

Aside from the historical definition, that originally considered BC only to photographic ($m_{\rm pg}$) or visual $m_{\rm V}$) magnitudes (Kuiper 1938), one can nowadays easily extend the definition to any waveband. A careful analysis of equation (2) makes clear some important properties of BC: (i) the value of $\mathcal{R}$ is a composite function of stellar fundamental parameters, namely $\mathcal{R} = \mathcal{R}(T_{\rm eff}, \log g, [X/H])$ so that, for fixed effective temperature, BC may display some dependence on stellar gravity (g) and chemical composition ($[X/H]$). (ii) The value of $\mathcal{R}$ (and, accordingly, of BC) is minimum when our observations catch the bulk of stellar luminosity. For this reason, high values of ${\rm BC}_V$ must be expected when observing for instance cool giant stars in the V band, or hot O-B stars in the infrared K band. (iii) The definition of the BC scale strictly depends on the assumed reference value for the Sun, which therefore must univocally fix the 'zero-point' of the scale (Bessell et al. 1998).

In this framework, we want to tackle here the central question of the possible BC dependence on stellar metallicity. This effect could be of special importance, in fact, in order to more confidently set the bolometric versus temperature scale for cool red giants, where the intervening absorption of diatomic (TiO *in primis*) and triatomic (H_2O) molecules heavily modulate the stellar SED with sizeable effects on optical and NIR magnitudes (e.g. Gratton et al. 1982; Bertone et al. 2008). As a matter of fact, still nowadays the many efforts devoted to the definition of the BC versus $\log T_{\rm eff}$ relationship led to non-univocal conclusions, with large discrepancies among the different sources in the literature as far as stars of K spectral type or later are concerned (Flower 1975, 1977; Bessell & Wood 1984; Houdashelt, Bell & Sweigart 2000; Bertone et al. 2004; Worthey & Lee 2006).

This issue actually has an even more important impact on the study of the integrated spectrophotometric properties of resolved and unresolved stellar systems, as red giants and other post-main-sequence (PMS) stars provide a prevailing fraction (2/3 or more; Buzzoni 1989) of the total luminosity of the population. A fair definition of the BC scale becomes, therefore, of paramount importance to self-consistently convert theoretical H–R and observed c–m diagrams of a stellar population (Flower 1996; VandenBerg & Clem 2003) and to more confidently assess the physical contribution of the different stellar classes.

A study of the BC dependence on metal abundance has been previously attempted by many authors mainly relying on a fully theoretical point of view to exploit the obvious advantage of stellar models to account, in a controlled way, for a global or selective change of metal abundance. In this regard, Tripicco & Bell (1995) and Cassisi et al. (2004), among others, tried to explore the effect of α elements enhancement (namely O, Mg, Ca, Ti etc.) in stellar SED, while Girardi et al. (2007) focused on the possible impact of helium abundance on BC. As a major drawback of these efforts, however, one has to report the admitted limitation of model atmospheres to accurately describe the spectrophotometric properties of K- and M-type stars, that are cooler than 4000 K (see Bertone et al. 2008, on this important point).

On the other hand, a fully empirical approach has been devised by Montegriffo et al. (1998) and Alonso et al. (1999), among others, trying to reconstruct stellar SED, and there from infer the bolometric flux, $f_{\rm bol}$, through optical broad-band photometry of stars in the Galactic field or in globular clusters. A recognized limitation of these studies is, however, that they may suffer from the lack of coverage of the stellar parameter space offered by the observations. Moreover, as far as the cool-star sequence is concerned, optical multicolour photometry, alone, partially misses the bulk of stellar emission (more centred towards the NIR spectral window); in addition, by converting broad-band magnitudes into monochromatic flux densities, the stellar SED is reconstructed at a very poor spectral resolution, thus possibly losing important features that may bias the inferred bolometric energy budget.

On this line, however, we want to further improve the analysis proposing here more complete spectroscopic observations for a large grid of red giant stars in several Galactic clusters along the entire metallicity scale from very metal-poor (i.e. [Fe/H] $\simeq -2.2$ dex)

[1] Recalling that emission peak roughly obeys the Wien law, i.e. $T\lambda_{\rm peak} \simeq$ const.

[2] For a more detailed analysis, note that the ratio $\mathcal{R}$ dimensionally matches the definition of 'equivalent width', and it gives a measure of how 'broad' is the whole SED compared to the monochromatic emission density at the reference λ.

Downloaded from https://academic.oup.com/mnras/article/403/3/1592/1050826 by INAF –IASF Bologna user on 17 January 2023

to supersolar ([Fe/H] $\simeq +0.4$ dex) stellar populations. Our observations span the whole optical and NIR wavelength range, thus allowing a quite accurate shaping of stellar SED. As we will demonstrate in the following discussion, our procedure allowed us to sample about 70–90 per cent of the total emission of our sample stars, thus leading to a virtually *direct* measure of $f_{\rm bol}$, even for M-type stars as cool as 3500 K.

We will arrange our discussion by presenting, in Section 2, our stellar data base together with further available information in the literature. The analysis of the observing material will be assessed in more detail in Section 3, while in Section 4 we will derive the SED for the whole sample leading to an estimate of the effective temperature and bolometric correction for each star. The discussion of the inferred BC–colour–temperature scale will be the focus of Section 5, especially addressing the possible dependence of BC on stellar metallicity. A comparison of our results with other relevant BC calibration in the literature will also be carried out in this section, while in Section 6 we will present the main conclusions of our work.

2 CLUSTER DATA BASE SELECTION

As we aim mainly at probing the impact of metallicity on the BC of stars at the low-temperature regime, a demanding constraint to set up our target sample was to explore a range as wide as possible in [Fe/H], and pick up red giant stars with accurate measurements of their metallicity. The cluster population in the Galaxy naturally provided the ideal environment for our task. By combining globular and open clusters, one can easily span the whole metallicity range pertinent to Population I and II stars in our and in external galaxies. We therefore selected five template systems, namely the three metal-poor globular clusters M15, M2 and M71, and two metal-rich open clusters, NGC 188 and NGC 6791, such as to let metallicity span almost three orders of magnitude, from [Fe/H] $= -2.3$ up to $+0.4$.

For each cluster, a subset of $\sim$20 suitable targets was then identified as among the brightest and coolest red giants from the 2MASS infrared c–m diagram (Skrutskie et al. 2006). In assembling the data set we also took care of picking up those objects from relatively uncrowded regions of the clusters, such as to reduce the chance of misidentification at the telescope.

The final set of target stars is summarized, for each cluster, in the five panels of Fig. 1 and in Tables 1–5. We eventually considered 92 stars in total, of which 21 are in M15, 18 in M2, 17 in M71, 16 in NGC 188 and 20 in NGC 6791, respectively. For each star, the tables always report the 2MASS id number (column 1) and the alternative cross-identification, according to other reference photometric catalogues, when available. The 2MASS J2000 coordinates on the sky and the corresponding J, H, K magnitudes are also always reported, together with a compilation of B, V, $R_{\rm C}$, $I_{\rm C}$ observed magnitudes according to the best reference catalogues for each cluster, as reported in the literature. When required, dereddened apparent magnitudes have been computed according to the colour excess $E(B-V)$ as labelled in the header of each table.

3 OBSERVATIONS AND DATA REDUCTION

Spectroscopic observations of our stellar sample have been collected during several runs between 2003 June and October at the 3.5-m Telecopio Nazionale Galileo (TNG) of the Roque de los Muchachos Observatory, at La Palma (Canary Islands, Spain). A summary of the logbook can be found in Table 6.

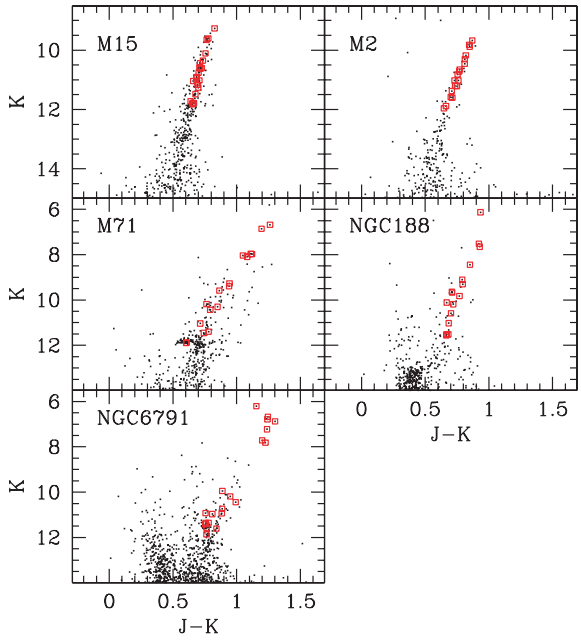

Figure 1. Apparent c–m diagram of the five clusters included in our analysis, according to 2MASS J and K photometry. Big squares along the red giant branch mark the selected targets in our sample.

Optical spectroscopy was carried out with the LRS FOSC camera; a composite spectrum was collected for each target by matching a blue (grism LRB along the $\lambda\lambda$3500–8800 Å wavelength range)[3] and a red set-up (grism LRR, $\lambda\lambda$4500–10 300 Å). In both cases the grisms provided a dispersion of 2.8 Å pixel^{-1} on a 2048 $\times$ 2048 thinned and back-illuminated Loral CCD, with a 13.5 μm pixel size. In order to collect the entire flux from target stars, we observed through a 5 arcsec wide slit; this condition actually made spectral resolution to be eventually constrained by the seeing figure (typically about 1–1.5 arcsec along the different nights), thus ranging between 10 and 15 Å [full width at half-maximum (FWHM)]. This is equivalent to a value of $R = \lambda/\Delta\lambda$ of 600–1000. Whenever possible, and avoiding severe crowding conditions of the target fields, the longslit was located at the parallactic angle. Wavelength calibration and data reductions were performed following standard procedures.

The optical spectra have then been accompanied by the corresponding observations taken at infrared wavelength with the NICS camera at the Nasmyth focus of the TNG. The camera was coupled with a Rockwell 1024 $\times$ 1024 Hawaii-1 HgCdTe detector. We took advantage of NICS unique design using the Amici grism coupled with two slits 0.5 and 5 arcsec wide, the latter being used for a complete flux sampling of the target stars. The spectra cover the entire wavelength range of 8000 Å to 2.5 μm at a resolving power (for a 0.5 arcsec slit) varying between $R = 80$ and 140 along the spectrum. In acquiring the spectra, the background subtraction and flat-fielding correction were eased by a standard dithering procedure on target images, while the wavelength calibration directly derived from the standard reference table providing the dispersion relation of the system. The MIDAS ESO package, and specifically its LONGSLIT

[3]Although nominally extended to 9500 Å, LRB spectra result is severely affected by second-order spectral emission in their red tail. For this reason, during data reduction, spectra have been clipped, retaining only the wavelength region blueward of 8800 Å.

Downloaded from https://academic.oup.com/mnras/article/403/3/1592/1050826 by INAF –IASF Bologna user on 17 January 2023

Table 1. Cluster properties and stellar data base for cluster M15.

M15:			$E(B-V)=0.10$				[Fe/H] $=-2.26$					
ID			α	δ	B	V		I_C		J	H	K
[a]	[b]	[c]	(J2000.0)		[b]	[b]	[c]	[b]	[c]	[a]	[a]	[a]
21300002+1209182	165	71	21:30:00.02	12:09:18.24	15.334	14.395	14.3460	13.330	13.2709	12.479	11.926	11.824
21295705+1208531	959	6	21:29:57.06	12:08:53.11	14.549	13.426	13.4946	12.144	12.2129	11.282	10.691	10.573
21295532+1210327	337	60	21:29:55.33	12:10:32.80	15.229	14.313	14.3694	13.165	13.2132	12.452	11.899	11.786
21300090+1208571	558	461	21:30:00.91	12:08:57.13	14.092	12.700	12.9683	11.281	11.4637	10.383	9.759	9.605
21295473+1208592	330	25	21:29:54.73	12:08:59.24	14.821	13.691	13.7581	12.444	12.5006	11.591	11.065	10.906
21300461+1210327	369		21:30:04.62	12:10:32.73	14.851	13.836				11.858	11.272	11.165
21295560+1212422	533	665	21:29:55.61	12:12:42.29	14.562	13.459	13.5218		12.2237	11.336	10.723	10.609
21300514+1210041	372		21:30:05.15	12:10:04.18	15.186	14.288				12.430	11.929	11.776
21295836+1209020		166	21:29:58.37	12:09:02.01			13.8205		12.5987	11.700	11.112	11.042
21295618+1210179		631	21:29:56.18	12:10:17.93			12.7694		11.3768	10.414	9.781	9.649
21295739+1209056		7	21:29:57.39	12:09:05.69			13.7397		12.5054	11.632	11.070	10.948
21300097+1210375		65	21:30:00.98	12:10:37.60			13.8739		12.6289	11.726	11.171	11.017
21300431+1210561	368		21:30:04.32	12:10:56.16	14.649	13.559				11.459	10.893	10.757
21301049+1210061	621		21:30:10.49	12:10:06.18	14.563	13.406				11.151	10.562	10.438
21300739+1210330	604		21:30:07.40	12:10:33.06	14.961	13.986				11.964	11.399	11.264
21300569+1210156			21:30:05.70	12:10:15.68						12.156	11.596	11.480
21300553+1208553			21:30:05.54	12:08:55.35						12.357	11.835	11.719
21295756+1209438			21:29:57.57	12:09:43.85						10.096	9.429	9.269
21295082+1211301			21:29:50.83	12:11:30.18						11.326	10.725	10.612
21295881+1209285		59	21:29:58.82	12:09:28.59			14.5465		13.5061	11.088	10.568	10.353
21295716+1209175		273	21:29:57.17	12:09:17.52			13.1662		11.7880	10.867	10.220	10.112

[a]From 2MASS.
[b]From Cohen, Briley & Stetson (2005).
[c]From Rosenberg et al. (2000).

Table 2. Cluster properties and stellar data base for cluster M2.[a]

M2:			$E(B-V)=0.06$		[Fe/H] $=-1.62$	
ID	α	δ	J	H	K	
	(J2000.0)					
21333827−0054569	21:33:38.28	−00:54:56.92	10.542	9.827	9.672	
21333095−0052154	21:33:30.96	−00:52:15.47	11.568	10.952	10.814	
21332468−0044252	21:33:24.69	−00:44:25.21	12.549	12.006	11.886	
21331771−0047273	21:33:17.71	−00:47:27.31	10.665	9.961	9.821	
21331723−0048171	21:33:17.24	−00:48:17.10	11.112	10.429	10.301	
21331790−0048198	21:33:17.91	−00:48:19.82	11.746	11.103	11.017	
21331854−0051563	21:33:18.55	−00:51:56.33	11.779	11.137	11.019	
21331948−0051034	21:33:19.49	−00:51:03.42	11.963	11.299	11.214	
21331923−0049058	21:33:19.23	−00:49:05.84	12.280	11.695	11.579	
21332588−0046004	21:33:25.89	−00:46:00.44	12.313	11.756	11.600	
21333668−0051058	21:33:36.68	−00:51:05.89	10.730	10.026	9.880	
21333520−0046089	21:33:35.21	−00:46:08.91	10.993	10.324	10.174	
21333488−0047572	21:33:34.88	−00:47:57.25	11.265	10.589	10.455	
21333593−0049224	21:33:35.94	−00:49:22.44	11.420	10.750	10.650	
21333432−0051285	21:33:34.33	−00:51:28.50	11.490	10.828	10.722	
21332531−0052511	21:33:25.32	−00:52:51.17	11.938	11.300	11.203	
21333109−0054522	21:33:31.09	−00:54:52.28	12.086	11.526	11.376	
21333507−0051097	21:33:35.07	−00:51:09.72	12.609	12.056	11.962	

[a]All the data are from 2MASS.

routine set, has been used for the whole reduction procedure, both for optical and infrared spectra.

3.1 Flux calibration

Given the nature of our investigation, special care has been devoted to suitably fluxing both optical and infrared spectra. This has been carried out by repeated observations, both with LRS and NICS, of a grid of spectrophotometric standard stars from the list of Massey et al. (1988) and Hunt et al. (1998), as reported in Table 6. Note, however, that the lack of an appropriate SED calibration of standard stars along the entire wavelength range of our observations required a two-step procedure, relying on the direct observation of Vega as a primary calibrator, according to Tokunaga & Vacca (2005) results. Given the outstanding luminosity of this star we had to observe through a 10 mag neutral filter to avoid CCD saturation, and create

Downloaded from https://academic.oup.com/mnras/article/403/3/1592/1050826 by INAF –IASF Bologna user on 17 January 2023

Table 3. Cluster properties and stellar data base for cluster M71.

M71:			$E(B-V)=0.25$				[Fe/H] $=-0.73$				
ID			α	δ	B	V		I_C	J	H	K
[a]	[b]	[c]	(J2000.0)		[b]	[b]	[c]	[c]	[a]	[a]	[a]
19535325+1846471	2672	256	19:53:53.25	18:46:47.13	13.905	12.314	12.2085	10.3988	9.090	8.197	8.040
19534750+1846169	2222	540	19:53:47.51	18:46:16.99	14.431	13.137	13.0010	11.5156	10.452	9.698	9.588
19535150+1848059	2541	892	19:53:51.50	18:48:05.91	14.079	12.436	12.3250	10.4275	9.079	8.207	7.968
19535064+1849075	2461	331	19:53:50.64	18:49:07.52	14.466	13.064	12.9955	11.4204	10.215	9.446	9.271
19534575+1847547	2079	648	19:53:45.76	18:47:54.80	14.247	12.606	12.4924	10.5109	9.094	8.203	7.974
19534827+1848021	2281	309	19:53:48.27	18:48:02.17	14.078	12.492	12.3636	10.5500	9.177	8.270	8.094
19534656+1847441	2145	46	19:53:46.57	18:47:44.19	14.838	13.623	13.5524	12.2176	11.228	10.569	10.435
19535369+1846039	2711	172	19:53:53.70	18:46:03.98	15.527	14.578	14.4974	13.3402	12.500	11.998	11.896
19534905+1846003	2337	303	19:53:49.05	18:46:00.34	14.601	13.410	13.3436	11.9991	10.950	10.276	10.186
19534916+1846512	2347	6	19:53:49.16	18:46:51.22	14.997	13.709	13.6219	12.2031	11.151	10.434	10.301
19534178+1848384	1772		19:53:41.79	18:48:38.46	15.877	14.694			12.183	11.521	11.402
19535676+1845399	2921		19:53:56.77	18:45:39.95	15.747	14.605			12.197	11.529	11.455
19533962+1848569	1611		19:53:39.62	18:48:56.99	15.695	14.627			12.494	11.974	11.888
19533864+1847554	1543		19:53:38.64	18:47:55.45	15.475	14.222			11.751	11.151	11.037
19534615+1847261		580	19:53:46.15	18:47:26.11			13.1140	11.5109	10.336	9.543	9.395
19535610+1847167	2885	1066	19:53:56.10	18:47:16.76	13.577	11.905	12.4009	9.2167	7.943	7.078	6.681
19534941+1844269	2365		19:53:49.41	18:44:26.98	13.863	12.107			8.058	7.105	6.863

[a]From 2MASS.
[b]From Geffert & Maintz (2000).
[c]From Rosenberg et al. (2000).

Table 4. Cluster properties and stellar data base for NGC 188.

NGC 188:			$E(B-V)=0.082$						[Fe/H] $=-0.02$				
ID			α	δ	B		V		R_C	I_C	J	H	K
[a]	[b]	[c]	(J2000.0)		[b]	[c]	[b]	[c]	[c]	[c]	[a]	[a]	[a]
00445253+8514055	4668	N188-I-69	00:44:52.54	85:14:05.54	13.613	13.579	12.319	12.357	11.598	11.087	10.098	9.461	9.304
00475922+8511322	5887	N188-II-181	00:47:59.23	85:11:32.28	13.587	13.428	12.135	12.197	11.429	10.894	9.891	9.203	9.100
00465966+8513157	5085	N188-I-105	00:46:59.66	85:13:15.71	13.603	13.538	12.362	12.422	11.732	11.269	10.349	9.789	9.639
00453697+8515084	5927	N188-I-57	00:45:36.97	85:15:08.43	14.799	14.760	13.658	13.706	13.039	12.571	11.709	11.149	11.024
00442946+8515093	4636	N188-I-59	00:44:29.46	85:15:09.39	14.986	14.950	14.005	14.046	13.385	12.962	12.202	11.653	11.520
00473222+8511024	5133	N188-II-187	00:47:32.22	85:11:02.45	15.171	15.132	14.077	14.140	13.490	...	12.234	11.700	11.567
00554526+8512209	6175		00:55:45.27	85:12:20.92	12.224	...	10.834	...	...	...	8.441	7.631	7.520
00463920+8523336	4843		00:46:39.21	85:23:33.67	12.890	...	11.569	...	...	...	9.292	8.597	8.441
00472975+8524140	4829		00:47:29.76	85:24:14.09	13.965	...	12.781	...	...	...	10.783	10.210	10.114
00441241+8509312	4756		00:44:12.42	85:09:31.23	12.933	...	11.404	...	...	...	8.580	7.892	7.652
00432696+8509175	4408		00:43:26.96	85:09:17.58	14.242	...	13.199	...	...	...	11.293	10.706	10.591
00471847+8519456	4909		00:47:18.48	85:19:45.65	14.255	...	13.010	...	...	...	10.908	10.289	10.187
00461981+8520086	4524		00:46:19.81	85:20:08.61	13.663	...	12.468	...	...	...	10.385	9.816	9.674
00463004+8511518	5894		00:46:30.05	85:11:51.89	15.142	...	14.052	...	...	...	12.185	11.695	11.518
00490560+8526077	5835		00:49:05.60	85:26:07.77	13.921	...	12.717	...	...	...	10.594	9.956	9.825
00420323+8520492	≡ SAO 109		00:42:03.23	85:20:49.23	11.40[d]		9.89[d]		...	...	7.064	6.387	6.130

[a]From 2MASS.
[b]From Platais et al. (2003).
[c]From Stetson, McClure & VandenBerg (2004).
[d]B and V photometry from SIMBAD.

a secondary calibrator (namely HD 192281) observed both with and without the neutral density filter.

Concerning the applied correction for atmosphere absorption, we had to manage two delicate problems. From one hand, in fact, the intervening action of Sahara dust (the so-called 'calima effect') may abruptly increase the atmosphere opacity at optical wavelength. This is a recurrent feature for summer nights at La Palma, and it can severely affect the observing output, especially when dealing with absolute flux calibration. A careful check with repeated observations of the same standard stars along each night allowed us to assess the presence of dust in the air. This confirmed, for instance, that along our observing runs, the night of 2003 August 7, displayed an outstanding (i.e. a factor of 4 higher than the average) dust extinction.

On the other hand, atmospheric water vapour can also play a role by affecting in unpredictable ways the infrared observations. Telluric H_2O bands about 1.10, 1.38 and 1.88 μm (Manduca & Bell 1979; Fuensalida & Alonso 1998), just restraining to the Amici wavelength range, may in fact strongly contaminate the *intrinsic* H_2O absorption bands of stellar SED, especially for stars cooler

Downloaded from https://academic.oup.com/mnras/article/403/3/1592/1050826 by INAF –IASF Bologna user on 17 January 2023

Table 5. Cluster properties and stellar data base for cluster NGC 6791.

NGC 6791:			$E(B-V)=0.117$									
ID			α	δ	B		V		I_C	J	H	K
[a]	[b]	[c]	(J2000.0)		[b]	[c]	[b]	[c]	[c]	[a]	[a]	[a]
19210807+3747494	6697	3475	19:21:08.07	37:47:49.41	15.279	15.275	13.909	13.978	12.668	11.675	11.071	10.919
19204971+3743426	10 807	3502	19:20:49.72	37:43:42.67	15.554	15.563	13.956	13.982	10.990	9.041	8.167	7.815
19205259+3744281	10 140	2228	19:20:52.60	37:44:28.18	15.715	15.732	14.095	14.150	12.397	11.135	10.417	10.185
19205580+3742307	11 799	3574	19:20:55.81	37:42:30.75	16.307	16.297	14.934	14.957	13.609	12.622	11.993	11.860
19205671+3743074	11 308	2478	19:20:56.72	37:43:07.46	16.000	15.984	14.633	14.660	13.325	12.351	11.756	11.586
19210112+3742134	12 010	3407	19:21:01.12	37:42:13.45	15.942	15.928	14.433	14.455	12.901	11.821	11.130	10.938
19211606+3746462	7750		19:21:16.06	37:46:46.26	15.472		13.871			8.914	8.053	7.714
19213656+3740376	12 650		19:21:36.56	37:40:37.63	15.727		14.174			11.431	10.635	10.438
19210326+3741190	13 637		19:21:03.27	37:41:19.04	15.722		14.348			12.120	11.516	11.362
19213635+3739445	13 082		19:21:36.36	37:39:44.57	16.186		14.825			12.449	11.728	11.608
19212437+3735402	15 790		19:21:24.37	37:35:40.29	15.837		14.442			12.134	11.546	11.354
19212674+3735186			19:21:26.75	37:35:18.60						11.622	10.925	10.735
19211632+3752154	3254		19:21:16.32	37:52:15.46	15.282		13.998			11.776	11.068	10.967
19211176+3752459	2970		19:21:11.76	37:52:46.00	15.676		14.336			12.174	11.557	11.420
19202345+3754578	1829		19:20:23.45	37:54:57.82	14.592		12.866			8.029	7.133	6.787
19205149+3739334			19:20:51.50	37:39:33.44						7.356	6.516	6.201
19203285+3753488	2394		19:20:32.85	37:53:48.87	15.056		13.417			8.463	7.535	7.224
19200641+3744452	9800		19:20:06.42	37:44:45.28	14.670		13.307			10.831	10.094	9.943
19200882+3744317	10 034		19:20:08.83	37:44:31.71	15.353		13.710			7.916	6.989	6.670
19203219+3744208	10 223		19:20:32.20	37:44:20.81	16.421		14.854			8.176	7.262	6.874

[a]From 2MASS.
[b]From Kaluzny & Rucinski (1995).
[c]From Stetson, Bruntt & Grundahl (2003).

Table 6. Logbook of TNG observations along 2003.

Obs. date (2003)	Instrument	Targets	Standards[a]
July 29	LRS	NGC 6791	HD 192281
July 30	LRS	NGC 6791	HD 192281, SAO 48300, WOLF 1346
July 31	LRS	NGC 6791	HD 192281, SAO 48300, WOLF 1346
August 6	LRS	M71	HD 192281, SAO 48300, WOLF 1346
August 7	LRS	M15	HD 192281, SAO 48300, WOLF 1346
August 11	NICS		HD 192281, SAO 48300
August 12	NICS		Vega
August 18	NICS	M71	HD 192281
August 19	NICS		Vega
August 20	NICS	M15, M71, NGC 188	HD 192281, SAO 48300, WOLF 1346, Vega
August 21	LRS	M2	HD 192281
August 23	LRS	M2, M15	HD 192281
August 26	LRS	NGC 188	
August 27	LRS	NGC 188	HD 192281
August 31	NICS	M71	HD 192281
September 1	NICS	M71, NGC 6791	HD 192281
September 3	NICS	M2, M15, NGC 188	SAO 48300
September 4	NICS	NGC 188	HD 192281
September 5	NICS	NGC 188, NGC 6791	HD 192281
October 14	NICS	M15	HD 192281
October 15	NICS	M2	HD 192281

[a]HD 192281 and WOLF 1346 from optical calibration by Massey et al. (1988); SAO 48300 from *JHK* photometric calibration by Hunt et al. (1998); Vega from Tokunaga & Vacca (2005).

than 3500 K (Bertone et al. 2008). This effect may act on short time-scales along the night, so that it cannot be reconducted to an average nightly extinction curve, as for optical observations. The H_2O contamination in each spectrum was therefore corrected by rescaling the average extinction curve to minimize the residual water vapour feature in the stellar spectra.

Overall, the full calibration procedure led us to consistently assemble the LRB–LRR–Amici spectral branches and obtain a

© 2010 The Authors. Journal compilation © 2010 RAS, MNRAS **403,** 1592–1610

Downloaded from https://academic.oup.com/mnras/article/403/3/1592/1050826 by INAF –IASF Bologna user on 17 January 2023

nominal SED of target stars along the 3450–25 000 Å wavelength range. However, just an eye inspection of the full spectra made evident in some cases a residual systematic component causing a 'glitch' at the boundary connection between LRS and NICS observations. Clearly, this effect urged us to further refine our analysis, taking into account the supplementary photometric piece of information, as we will discuss in more detail in the next section.

3.2 Photometry and spectral 'fine tuning'

The relevant data base of broad-band photometry available in the literature for all stars in our sample can be usefully accounted for in our analysis as a supplementary tool to tackle the inherent difficulty in reproducing the overall shape of stellar SED at the required accuracy level over the entire range of our observations.

As summarized in Tables 1–5, a wide collection of photometric catalogues can be considered, providing multicolour photometry along the range spanned by LRS and NICS spectra. Facing the observed values, one can similarly derive a corresponding set of multicolour synthetic magnitudes relying on the assembled SED of each star. Operationally, from our $f(\lambda)$ values we need to numerically assess the quantity

$$m^j_{\rm syn} = -2.5\ \log \frac{\int f(\lambda) S(\lambda)^j\ {\rm d}\lambda}{\int S(\lambda)^j\ {\rm d}\lambda} - 2.5\ \log f^j_0 \qquad (3)$$

being $m^j_{\rm syn}$ the synthetic magnitude in the jth photometric band, identified by a filter response $S(\lambda)^j$ and a calibrating zero-point flux f^j_0. For our calculations we relied on the Buzzoni (2005) reference data (see table 1 therein).

A comparison of our output with the available photometry is displayed in Fig. 2. The magnitude difference (in the sense 'synthetic' − 'observed') is plotted in the different panels of the figure versus *observed* colour, according to the different photometric catalogues quoted in Tables 1–5. As typically two sources for V magnitudes are available for most clusters, the observed colours have been computed for each available V data set and are displayed with a different marker (either dot or square) in the plots.

Just a glance to Fig. 2 makes it evident that systematic offsets are present between observed photometry and synthetic magnitudes. This may partly be due to zero-point uncertainty in computing equation (3), as well as to residual systematic drifts inherent to our spectral flux calibration. In addition, from the figure one has also to report a few outliers in every band, and a notably skewed distribution of B residuals. To recover for this systematics, we devised an iterative 3σ clipping procedure on the data of Fig. 2 to reject deviant stars and lead synthetic magnitudes to match the standard photometric system of the observed catalogues. Our results are displayed in graphical form in the plots of Fig. 3.

After just a few rejections, our procedure quickly converged to mean magnitude offsets ($\langle$obs − syn$\rangle$; see Table 7) to correct equation (3) output. After correction for this systematics, our final synthetic photometry of cluster stars (not accounting for Galactic reddening) is collected in Tables 8 and 9. According to Table 7, note that a $\sigma = 0.095$ mag in total magnitude residuals evidently implies an *internal* accuracy in our spectral flux calibration of target stars better than 10 per cent.

3.3 Stellar outliers

It could be interesting to analyse in some detail the deviant stars in our Δm clipping procedure in order to collect further clues about their nature. Apart from the obvious impact of photometric errors,

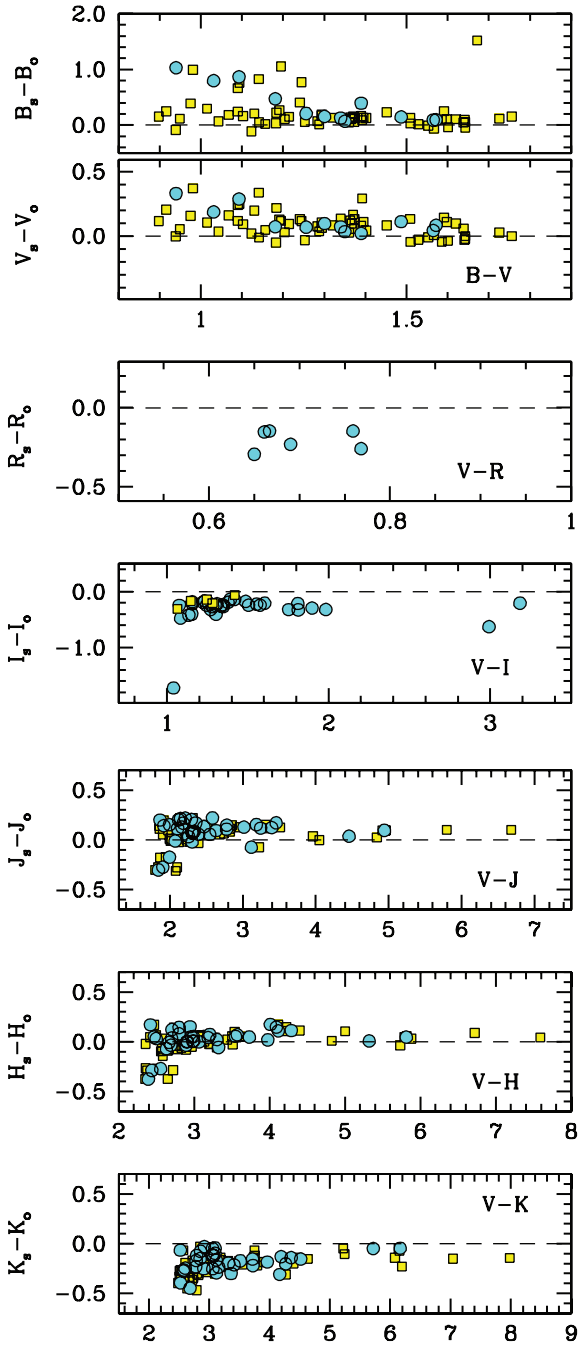

Figure 2. The B, V, $R_{\rm C}$, $I_{\rm C}$, J, H, K magnitude residuals between synthetic and observed magnitudes (in the sense 'syn' − 'obs') for the 94 stars in our sample, plotted versus literature colours, according to the data of Tables 1–5. Synthetic magnitudes derived from the numerical integration of the observed SED with the Johnson–Cousins filters. All the available photometry has been accounted for. Some stars with multiple V data sets appear, therefore, twice in the plots and are singled out by dot and square markers, respectively.

3σ outliers may in fact more likely be displaying signs of an intrinsic physical variability in their luminosity.

As summarized in Table 10, in total 10 stars have been found to significantly ($>3\sigma$) deviate from the literature compilations. A careful check of their identifications on the SIMBAD data base indicates that at least three of them are known variables (typically

Downloaded from https://academic.oup.com/mnras/article/403/3/1592/1050826 by INAF –IASF Bologna user on 17 January 2023

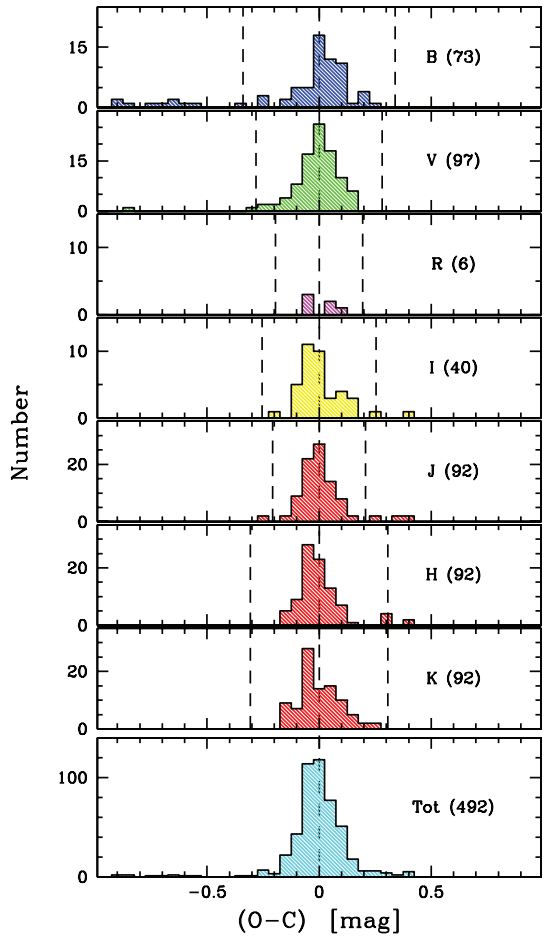

Figure 3. The histogram of magnitude residuals for the data of Fig. 2, after correction for the systematic offsets, according to Table 7. A total of 492 measures have been accounted for, as labelled in the global histogram of the bottom panel, including multiple photometry sources in the literature from Tables 1–5. Dashed vertical lines mark the $\pm 3\sigma$ clipping edges, according to our iterative procedure, as devised in Section 3.2. Mag residuals are in the sense 'obs' − 'syn'. After outliers rejections, the global sample of 458 measurements has, on average, $\sigma(\Delta\text{mag}) = \pm 0.095$ (see Table 7).

Table 7. Magnitude residuals between observed and theoretical magnitudes.[a]

	All the clusters			
Band	⟨obs − syn⟩	σ	$N_{\rm in}$	$N_{\rm out}$
B	−0.137	0.113	63	10
V	−0.091	0.094	72	1
$R_{\rm C}$	+0.205	0.065	6	–
$I_{\rm C}$	+0.244	0.085	38	2
J	−0.093	0.069	88	9
H	−0.012	0.102	94	3
K	+0.197	0.102	97	–
Total	0.000[b]	0.095	458	25

[a]Magnitude residuals are in the sense of observed − synthetic one.
[b]Weighting with the number of entries, $N_{\rm in}$.

semiregulars or irregulars, as expected for their nature of late-type red giants).[4] No firm conclusions can be drawn, on the contrary, for the other seven cases, although it is evident even from a colour check (see Fig. 4) that they have been picked up in an intrinsically different status with respect to previous data in the literature.[5] We therefore commend the stars in the list of Table 10 as special candidates for further in-depth investigations for variability.

4 SPECTRAL ENERGY DISTRIBUTION AND BOLOMETRIC LUMINOSITY

The synthetic photometric catalogues obtained from the observed spectral data base had a twofold aim: first, this procedure allowed us to self-consistently match broad-band magnitudes with the inferred measure of $m_{\rm bol}$ in order to obtain the corresponding value of the bolometric correction; secondly, the study of the magnitude residuals with respect to the literature data provided us with the appropriate offsets in flux rescaling such as to 'smoothly' connect our optical and infrared spectra and lead therefore to a more accurate estimate of $m_{\rm bol}$.

Operationally, for the latter task, we proceeded as follows. Taking into account the individual set of ⟨obs − syn⟩ magnitude residuals, for each star in our sample we computed a mean optical and infrared offset ($\Delta m_{\rm LRS}$ and $\Delta m_{\rm NICS}$, respectively) by separately averaging the B, V, $R_{\rm C}$, $I_{\rm C}$ and J, H, K mag residuals. The LRS spectra and the NICS observations have then been matched by multiplying visual and IR fluxes by a factor of $10^{-0.4\,(\Delta m_{\rm LRS})}$ and $10^{-0.4\,(\Delta m_{\rm NICS})}$, respectively. Foreground reddening has been corrected relying on the standard relation $k(\lambda) = A(\lambda)/E(B-V)$ (Scheffler 2006), where the appropriate value of the colour excess $E(B-V)$ is from the headers of Tables 1–5. In its final form, the SED is reshaped such as $f_0(\lambda) = f(\lambda)\, 10^{0.4\,k(\lambda)E(B-V)}$.

The LRS and NICS spectra have been connected at 8800 Å, by smoothing the wavelength region between 7800 and 10 000 Å (in order to gain S/N, especially for LRS poor signal at the long wavelength edge). In Fig. 5, we summarize our results for an illustrative set of SEDs by picking up for each cluster the brightest (i.e. roughly the coolest) and faintest (i.e. warmest) stars in our sample.[6] Note, from the figure, the striking presence of the CO bump at about 1.6 μm (Frogel et al. 1978; Lançon & Mouhcine 2002), as well as the broad H_2O absorption bands to which the sharper (and variable) emission of telluric water vapour superposes (see, in particular, the case of M15 stars in the figure). This made far more difficult any accurate cleaning procedure, as we discussed in Section 3.1.

4.1 Temperature scale

Although sampled over a wide wavelength range, SED of our stars still lacks the contribution of ultraviolet and far-infrared luminosity.

[4]Note, on the other hand, the counter-example of star #2156 in NGC 6791, known as Irr variable V70 ≡ SBG 2240 (Mochejska, Stanek & Kaluzny 2003) and not a deviant in our spectroscopic observations.
[5]Curiously enough, however, one may note that six out of the seven remaining objects are all located in NGC 188, and are both B and J outliers. Both photometric bands actually cover the 'bluer' wavelength regions of both the LRS and NICS spectra, respectively. This coincidence might perhaps indicate some hidden problem with the flux calibration procedure during the observation of this cluster.
[6]For the interested reader, the entire spectral data base is available in electronic form upon request, or directly on the web at the authors' web site http://www.bo.astro.it/∼eps/home.html

Downloaded from https://academic.oup.com/mnras/article/403/3/1592/1050826 by INAF –IASF Bologna user on 17 January 2023

Table 8. Standard synthetic photometry from SED of target stars in globular clusters M71, M15 and M2.[a]

ID	B	V	R_C	I_C	J	H	K
			M15				
21300002+1209182	15.11	14.30	13.81	13.27	12.58	12.08	11.95
21295705+1208531	14.30	13.35	12.79	12.18	11.41	10.82	10.74
21295532+1210327	15.34	14.43	13.85	13.24	12.50	11.94	11.72
21300090+1208571	14.04	12.90	12.21	11.47	10.51	9.82	9.50
21295473+1208592	14.89	13.80	13.19	12.55	11.62	11.02	10.95
21300461+1210327	15.01	13.85	13.24	12.62	11.86	11.16	10.98
21295560+1212422	14.59	13.46	12.86	12.23	11.41	10.79	10.55
21300514+1210041	15.20	14.31	13.79	13.23	12.45	11.89	11.64
21295836+1209020	14.80	13.83	13.27	12.65	11.81	11.22	11.01
21295618+1210179	14.02	12.89	12.19	11.48	10.49	9.82	9.55
21295739+1209056	14.89	13.83	13.22	12.58	11.65	11.05	11.03
21300097+1210375	14.91	13.85	13.24	12.63	11.85	11.19	11.14
21300431+1210561	14.76	13.59	12.91	12.25	11.40	10.81	10.65
21301049+1210061	14.45	13.36	12.73	12.09	11.25	10.60	10.35
21300739+1210330	15.22	14.05	13.36	12.67	11.86	11.24	11.10
21300569+1210156	15.02	14.11	13.56	12.97	12.21	11.61	11.50
21300553+1208553	15.82	14.84	14.26	13.61	12.50	11.86	11.65
21295756+1209438	13.80	12.45	11.72	11.01	10.10	9.47	9.32
21295082+1211301	14.61	13.52	12.91	12.27	11.40	10.82	10.66
21295881+1209285[b]	14.62	13.40	12.70	12.03	11.17	10.57	10.42
21295716+1209175	13.96	13.03	12.45	11.84	10.98	10.36	10.20
			M2				
21333827−0054569	13.71	12.72	12.17	11.58	10.55	9.85	9.73
21333095−0052154	14.74	13.68	13.11	12.53	11.59	10.96	10.87
21332468−0044252	15.71	14.65	14.07	13.48	12.59	12.01	11.94
21331771−0047273	14.30	13.02	12.32	11.66	10.69	9.94	9.91
21331723−0048171	15.06	13.66	12.91	12.21	11.18	10.44	10.32
21331790−0048198	15.87	14.74	14.17	13.54	12.00	11.05	10.90
21331854−0051563	14.88	13.89	13.32	12.72	11.80	11.17	11.06
21331948−0051034	15.11	14.12	13.55	12.93	12.01	11.38	11.17
21331923−0049058	16.49	15.21	14.58	13.91	12.52	11.67	11.46
21332588−0046004	15.42	14.44	13.89	13.33	12.40	11.78	11.59
21333668−0051058	14.35	13.12	12.47	11.81	10.76	10.05	9.92
21333520−0046089	14.58	13.36	12.70	12.04	11.02	10.34	10.23
21333488−0047572	14.98	13.67	12.98	12.30	11.33	10.64	10.42
21333593−0049224	15.31	13.93	13.18	12.48	11.49	10.82	10.60
21333432−0051285	14.89	13.72	13.09	12.45	11.50	10.87	10.77
21332531−0052511	15.26	14.11	13.51	12.90	11.98	11.38	11.18
21333109−0054522	15.98	14.57	13.80	13.08	12.15	11.56	11.37
21333507−0051097	15.94	14.78	14.14	13.52	12.63	12.07	12.02
			M71				
19535325+1846471	14.02	12.37	11.42	10.43	8.92	8.36	7.93
19534750+1846169	14.48	13.11	12.36	11.59	10.41	9.71	9.57
19535150+1848059	13.99	12.32	11.34	10.38	9.10	8.30	8.02
19535064+1849075	14.46	13.02	12.22	11.42	10.27	9.49	9.25
19534575+1847547	14.21	12.48	11.45	10.43	9.12	8.30	8.02
19534827+1848021	14.04	12.36	11.40	10.47	9.24	8.41	8.09
19534656+1847441	14.85	13.63	12.93	12.21	11.22	10.56	10.47
19535369+1846039	15.50	14.54	14.01	13.40	12.56	12.02	11.85
19534905+1846003	14.73	13.45	12.75	12.01	10.91	10.26	10.15
19534916+1846512	14.87	13.65	13.01	12.30	11.19	10.46	10.30
19534178+1848384	15.77	14.55	13.87	13.17	12.24	11.58	11.40
19535676+1845399	15.66	14.50	13.86	13.18	12.22	11.58	11.43
19533962+1848569	15.74	14.70	14.13	13.50	12.50	11.87	11.74
19533864+1847554	15.39	14.10	13.42	12.72	11.72	11.19	11.09
19534615+1847261	14.68	13.21	12.38	11.55	10.35	9.60	9.44
19535610+1847167[c]	14.96	13.27	11.21	9.26	7.89	7.08	6.83
19534941+1844269[d]	13.88	12.02	10.71	9.42	7.96	7.20	6.96

[a] After correction for the systematic offsets, according to Table 7.
[b] Dropped: *I* outlier.
[c] Dropped: SR variable Z Sge; *B*, *V* outlier.
[d] Var AN 48.1928 (Baade 1928).

Downloaded from https://academic.oup.com/mnras/article/403/3/1592/1050826 by INAF –IASF Bologna user on 17 January 2023

Table 9. Standard synthetic photometry from SED of target stars in open clusters NGC 188 and NGC 6791.[a]

ID	B	V	R_C	I_C	J	H	K
			NGC 188				
00445253+8514055	13.65	12.34	11.66	11.01	10.04	9.41	9.45
00475922+8511322	13.68	12.13	11.38	10.73	9.78	9.20	9.25
00465966+8513157	13.87	12.40	11.71	11.11	10.25	9.71	9.67
00453697+8515084[b]	15.49	13.90	13.10	12.40	11.44	10.87	10.77
00442946+8515093[c]	15.84	14.28	13.44	12.73	11.81	11.27	11.32
00473222+8511024[d]	15.79	14.24	13.40	12.73	11.87	11.40	11.49
00554526+8512209	12.25	10.82	10.06	9.34	8.31	7.59	7.54
00463920+8523336	12.89	11.56	10.87	10.21	9.19	8.53	8.50
00472975+8524140	14.05	12.91	12.33	11.74	10.70	10.11	9.98
00441241+8509312	12.81	11.28	10.45	9.68	8.60	7.85	7.78
00432696+8509175	14.17	13.14	12.61	12.08	11.25	10.76	10.59
00471847+8519456[e]	14.89	13.03	12.19	11.47	10.54	9.99	10.07
00461981+8520086[f]	14.58	12.50	11.60	10.88	9.98	9.43	9.40
00463004+8511518[g]	15.67	14.20	13.45	12.78	11.91	11.42	11.38
00490560+8526077	13.89	12.65	12.02	11.41	10.48	9.90	9.97
00420323+8520492	11.29	9.75	8.91	8.14	7.05	6.43	6.20
			NGC 6791				
19210807+3747494	15.29	13.98	13.33	12.70	11.66	11.06	10.87
19204971+3743426[h]	15.52	13.97	12.31	10.61	9.04	8.20	7.97
19205259+3744281	15.69	14.10	13.19	12.32	11.17	10.45	10.20
19205580+3742307	16.23	14.90	14.23	13.59	12.61	12.03	11.96
19205671+3743074	15.97	14.64	13.96	13.31	12.32	11.74	11.66
19210112+3742134	15.94	14.48	13.68	12.92	11.82	11.06	10.96
19211606+3746462	15.29	13.74	12.11	10.45	8.91	8.10	7.84
19213656+3740376	15.58	14.07	13.24	12.46	11.40	10.72	10.50
19210326+3741190	15.72	14.39	13.69	13.01	12.03	11.44	11.36
19213635+3739445	16.10	14.76	14.11	13.49	12.47	11.78	11.58
19212437+3735402	15.83	14.46	13.79	13.15	12.14	11.45	11.30
19212674+3735186	15.33	13.98	13.25	12.56	11.59	10.99	10.79
19211632+3752154	15.22	13.98	13.32	12.67	11.71	11.12	10.93
19211176+3752459	15.65	14.38	13.73	13.11	12.13	11.47	11.41
19202345+3754578	14.57	12.80	11.43	9.63	7.96	7.08	6.84
19205149+3739334	13.26	11.66	10.23	8.75	7.35	6.58	6.23
19203285+3753488	14.97	13.39	11.67	10.00	8.46	7.55	7.19
19200641+3744452	14.67	13.34	12.61	11.89	10.79	10.06	9.87
19200882+3744317	15.17	13.62	11.61	9.67	7.92	7.07	6.72
19203219+3744208[i]	16.22	14.77	12.46	10.23	8.18	7.29	6.93

[a] After correction for the systematic offsets, according to Table 7.
[b] Dropped: B, J outlier.
[c] Dropped: B, J, H outlier.
[d] Dropped: B, J outlier.
[e] Dropped: B, J outlier.
[f] Dropped: B, J, H outlier.
[g] Dropped: B, J outlier.
[h] Dropped: I outlier; V13 - Var? (de Marchi et al. 2007).
[i] V70 ≡ SBG 2240: Irr var (Mochejska et al. 2003).

Clearly, a safe assessment of this contribution is mandatory to lead to a confident measure of the bolometric magnitude. As the amount of energy released outside the spectral window of our observations critically depends on stellar temperature, our task to compute BC requires in fact a parallel calibration of $T_{\rm eff}$ in the range of our red giant stars.

Among the many outstanding efforts in this direction, we have to recall the works of Flower (1975), Bessell (1979), Blackwell, Petford & Shallis (1980), Ridgway et al. (1980), Bessell et al. (1998), Houdashelt et al. (2000), VandenBerg & Clem (2003), Bertone et al. (2004) and Worthey & Lee (2006). In their exhaustive analysis, Alonso et al. (1999) provided an accurate analytical set of fitting functions that calibrate stellar effective temperature versus Johnson/Cousins broad-band colours. The Alonso et al. (1999) calibration relies on the IRFM estimate of stellar surface brightness, and considers stars of spectral type K5 or earlier, spanning a wide metallicity range ($-3.0 \lesssim$ [Fe/H] $\lesssim +0.2$). Within this range, the Alonso et al. claim that the internal accuracy in the definition of $T_{\rm eff}$ is better than 5 per cent. As a further important result of their work, some colours, like $(V - I)$, $(V - L')$, $(J - K)$ and $(I - K)$ are found to be fair tracers of temperature, almost independently of stellar metallicity.

Downloaded from https://academic.oup.com/mnras/article/403/3/1592/1050826 by INAF –IASF Bologna user on 17 January 2023

Table 10. Stellar outliers of our sample in the different photometric bands.

Cluster	ID	Outlier in							Notes
		B	V	R_C	I_C	J	H	K	
M15	180	...	...	...	x	...	...	...	...
M71	4212	x	x	...	...	...	...	...	Z Sge - SRa P $\sim$ 175 d
	5755	...	...	...	x	...	...	...	V2 $\equiv$ AN 48.1928 - Ir
N188	567	x	...	...	...	x	...	...	...
	652	x	...	...	...	x	x	...	...
	1109	x	...	...	...	x	...	...	...
	630	x	...	...	...	x	...	...	...
	174	x	...	...	...	x	x	...	...
	1352	x	...	...	...	x	...	...	...
N6791	3502	...	...	...	x	...	...	...	V13 - Var?
Total		7	1	0	3	6	2	0	

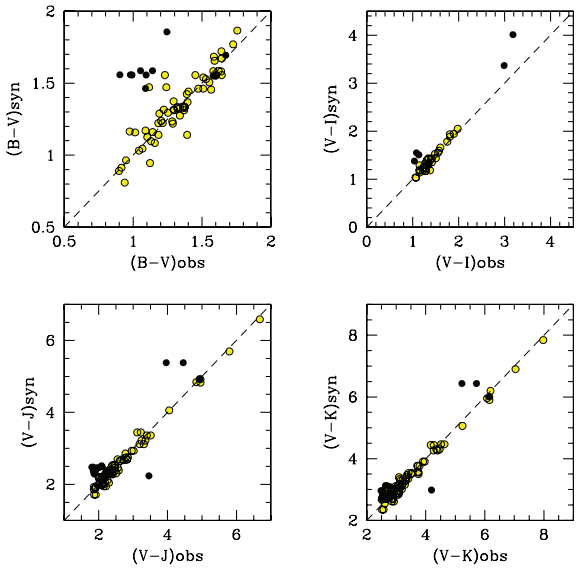

Figure 4. Colour distribution of photometric outliers, according to our 3σ clipping procedure (see Fig. 3). Target location for the whole star sample in the synthetic versus observed colour planes are displayed, with dark solid dots marking the 'dropped' objects (see Table 10).

The Alonso et al. (1999) calibration, however, applies strictly to stars warmer than ~4000 K, while our stellar sample definitely spans a wider colour range. This is certainly the case, for instance, of the brightest giant stars in NGC 6791, too (infra)red to match the Alonso et al. fitting functions. For these cases one could rely on the wider validity range of the $(B - V)$ calibration, although the advantage may only be a nominal one as any optical colour, like $(B - V)$, tends naturally to saturate when moving to $T_{\rm eff} \lesssim 4000$ K (Johnson 1966, see also fig. 2 in Alonso et al. 1999).

Considering the whole set of the Alonso et al. fitting functions, we eventually chose four reference colours to assess the value of effective temperature for our stars. Two colours, namely $(B - V)$ and $(J - K)$, are entirely comprised within the LRS and NICS spectral branches, respectively, and they can therefore ostensibly probe the shape of SED in a more self-consistent way. To these two colours we also added $(V - I_C)$ and $(V - K)$, as they provided a check of our flux calibration bridging the optical and infrared regions of the spectra.

Dereddened colours for each star in our sample eventually provided a set of nominal values of $T_{\rm eff}$, by entering the appropriate fitting functions. The 'allowed' values of $T_{\rm eff}$ (i.e. if comprised within the boundary limits of the adopted calibration functions) were then averaged, deriving the mean fiducial value of the effective temperature, reported in Tables 11 and 12 (column 10). In case of just one $T_{\rm eff}$ estimate [typically from $(J - K)$ colour], we also added the $(V - K)$ output (reported in italics in the tables) trusting on a fairly smooth trend of the Alonso et al. (1999) calibration for this colour, when extrapolated to cooler temperatures (see figs 8 and 10 therein).

Once combining the different temperature estimates from the four reference colours in our analysis, we report in Fig. 6 the resulting $T - \langle T \rangle$ distribution, considering the whole set of 322 individual residuals. The figure confirms that an unbiased estimate of $T_{\rm eff}$ may eventually be achieved with our procedure, within a ± 150 K uncertainty on the standard measure. As typically two to four useful temperature estimates are available from the colours of each star (see, again, Tables 11 and 12), we may expect final $T_{\rm eff}$ values for our sample to be assessed within a 70–100 K (i.e. 1–3 per cent) internal uncertainty.

4.2 Towards $m_{\rm bol}$

The fiducial effective temperature, as reported in column 10 of Tables 11 and 12, provided the reference quantity to constrain the unsampled fraction of stellar luminosity, outside the wavelength limits of our spectral observations. No univocal procedure can be devised to effectively tackle this problem. On one hand, in fact, both the ultraviolet and mid- and far-infrared stellar emission can in principle be modulated by a number of different mechanisms (mass loss and stellar winds, or circumstellar gas and dust lanes thermalizing ultraviolet and optical photons, photospheric spots, pulsating variability etc.). On the other hand, one would better like to proceed with a straight heuristic approach, such as to self-consistently size up the amount of 'overflown' luminosity and decide the accuracy level in its correction procedure, according to an 'ex-post' analysis of the results.

On this line, we therefore decided to proceed in the most straightforward way for each star, by extrapolating its observed SED to both ultraviolet and infrared windows by means of two blackbody branches, of appropriate (fixed) temperature $\langle T \rangle$ as given in Tables 11 and 12. The two spectral branches have been *separately* rescaled to the (dereddened) flux values of the observed SED by setting the boundary wavelengths respectively at 4000 and 22 500 Å; the integrated luminosity has then been computed within the three relevant regions of each stellar SED, identifying the

Downloaded from https://academic.oup.com/mnras/article/403/3/1592/1050826 by INAF –IASF Bologna user on 17 January 2023

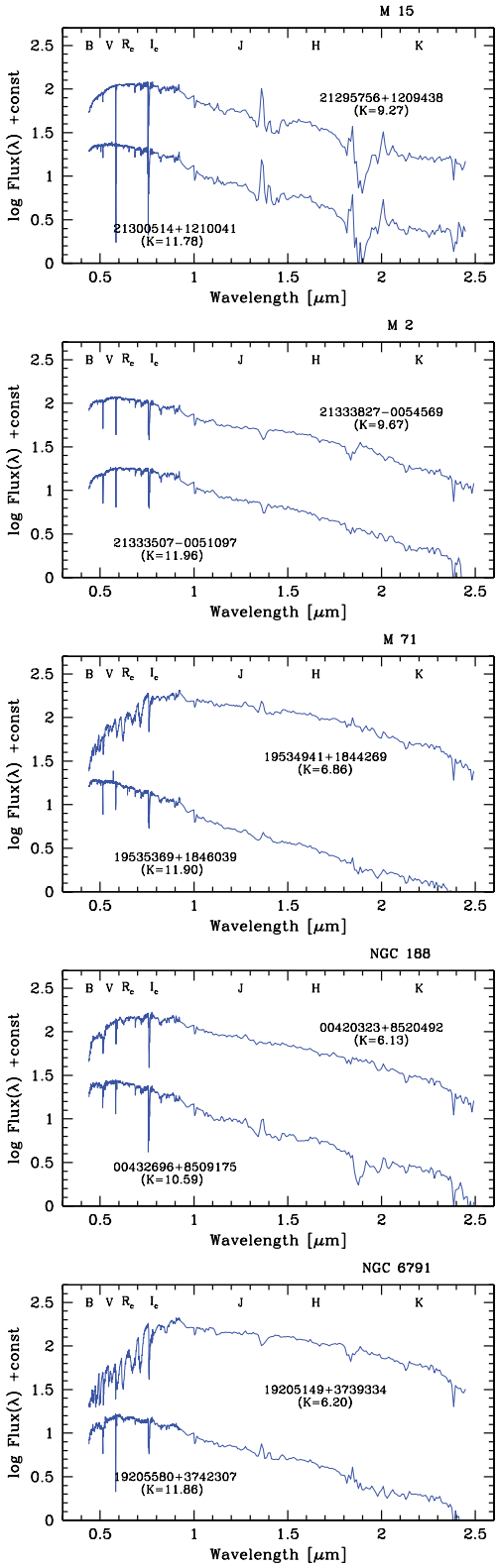

Figure 5. The resulting (dereddened) SED according to optical and infrared observations for an illustrative stellar subset of each cluster, including the brightest (and roughly coolest) and faintest (i.e. warmest) stars. Note, especially for the M15 stars, the strong impact of telluric water vapour bands at 1.38 and 1.88 μm. Their variability along the observing nights prevented, in some cases, any accurate cleaning procedure. See discussion in Section 3.1.

ultraviolet contribution $l_{\rm UV}$ (in $0 \leq \lambda \leq 4000$ Å) an optical/mid-infrared luminosity $l_{\rm obs}$ ($4000 \leq \lambda \leq 22\,500$ Å) and a far-infrared contribution $l_{\rm FIR}$ (longward of 2.25 μm). For comparison, the same exercise has been repeated for a straight blackbody spectral distribution exploring the luminosity fraction emitted shortward of $\lambda \leq 4000$ Å and longward of $\lambda \geq 22\,500$ Å along the temperature range of our sample.

Our results are summarized in Fig. 7. Compared to the blackbody approximation, real stars are brighter at longer wavelength and slightly fainter, on the contrary, at UV wavelength. In total, one sees from Fig. 7 that the fraction of 'lost' luminosity, namely $F_l = (l_{\rm bol} - l_{\rm obs})/l_{\rm bol}$, turns out to be about 15 per cent for the bulk of red giants in our sample; this figure can, however, quickly raise with decreasing temperature, and about one-third of bolometric luminosity might in fact be 'stored' at FIR wavelengths. Within these limits, and accounting for the 70–100 K internal uncertainty of our temperature scale, one sees from the Fig. 7 that $m_{\rm bol}$ can be secured for our sample stars within a few 0.01 mag uncertainty.[7]

Starting from the bolometric flux (which also includes the unsampled luminosity fraction, according to our procedure), the apparent magnitude for each star derives as $m_{\rm bol} = -2.5 \log f_{\rm bol} +$ Z.P. If we *assume* for the Sun an absolute $M_{\rm bol} = +4.72$, and $L_\odot = 3.89\,10^{33}$ erg s^{-1}, the bolometric zero-point directly derives as Z.P. $= -11.50$ mag. On the same line, the BC scale is fixed once adopting an observed value for the apparent V magnitude of the Sun. Following Lang (1991), if $m_{\rm V}^\odot = -26.78$, then $M_{\rm V}^\odot = +4.79$ and a $BC_{\rm V}^\odot = -0.07$ mag derives. Our output, for the whole stellar sample, is reported in column 11 of Tables 11 and 12, together with the relevant (dereddened) BC to the V and K photometric bands (BC_V and BC_K, respectively, in columns 12 and 13 of the tables).

5 RESULTS AND DISCUSSION

The data of Tables 11 and 12 are the main output of our analysis. According to our results, we can explore three relevant relationships, linking BC with the effective temperature of stars and with two reference colours like $(B - V)$ and $(V - K)$. Given the temperature range of red giants, it could be of special relevance to consider the K-band BC; however, for its more general interest, we will also include in our discussion the more standard case of the BC_V.

5.1 BC–colour–temperature relations

Like, for a colour–colour diagram, the BC versus colour relationship can be regarded as an *intrinsic* (i.e. distance-independent) feature characterizing the stellar SED. On the corresponding theoretical side, we also want to study here the resulting dependence of BC on stellar effective temperature, a relation that allows us to more directly match the observations with the theoretical predictions of stellar model atmospheres.

In a first set of plots (see Fig. 8), we display the observed distribution of our stars in the different planes. In order to single out any possible dependence on chemical composition of stars, we marked

[7]The claimed $m_{\rm bol}$ uncertainty simply derives as $\sigma \sim \partial F_l/\partial T_{\rm eff}\,\sigma(T_{\rm eff})$, where $\sigma(T_{\rm eff}) \lesssim 100$ K and the F_l derivative can be estimated from Fig. 7. In any case, it is clear from the figure that, by neglecting any further luminosity correction to our data for the unsampled luminosity, we would be overestimating $m_{\rm bol}$ by at most 0.3 mag.

Downloaded from https://academic.oup.com/mnras/article/403/3/1592/1050826 by INAF –IASF Bologna user on 17 January 2023

Table 11. Inferred temperatures, bolometric magnitude and bolometric corrections for target stars in globular clusters M71, M15 and M2.

ID	$(B-V)_o$	$(V-I_{C})_o$	$(V-K)_o$	$(J-K)_o$	T_{BV} (K)	T_{VI} (K)	T_{VK} (K)	T_{JK} (K)	$\langle T \rangle$ (K)	Bol_o	BC_V	BC_K
					M15							
21300002+1209182	0.71	0.87	2.08	0.58	5043	5039	5019	4748	4962	13.742	−0.25	1.83
21295705+1208531	0.85	1.01	2.34	0.62	4721	4711	4723	4619	4694	12.697	−0.34	1.99
21295532+1210327	0.81	1.03	2.44	0.73	4777	4669	4618	4307	4593	13.754	−0.37	2.07
21300090+1208571	1.04	1.27	3.13	0.96	4474	4242	4117	3806	4160	11.918	−0.67	2.45
21295473+1208592	0.99	1.09	2.58	0.62	4536	4549	4506	4619	4552	13.032	−0.46	2.12
21300461+1210327	1.06	1.07	2.60	0.83	4449	4588	4490	4068	4399	13.148	−0.39	2.20
21295560+1212422	1.03	1.07	2.64	0.81	4486	4588	4457	4113	4411	12.733	−0.42	2.22
21300514+1210041	0.79	0.92	2.40	0.76	4827	4915	4660	4231	4658	13.674	−0.33	2.07
21295836+1209020	0.87	1.02	2.55	0.75	4694	4690	4532	4256	4543	13.102	−0.42	2.13
21295618+1210179	1.03	1.25	3.07	0.89	4486	4272	4153	3941	4213	11.934	−0.65	2.42
21295739+1209056	0.96	1.09	2.53	0.57	4574	4549	4549	4782	4614	13.068	−0.45	2.07
21300097+1210375	0.96	1.06	2.44	0.66	4574	4608	4618	4499	4575	13.135	−0.41	2.03
21300431+1210561	1.07	1.18	2.67	0.70	4437	4386	4433	4387	4411	12.798	−0.48	2.18
21301049+1210061	0.99	1.11	2.74	0.85	4536	4511	4378	4024	4362	12.586	−0.46	2.27
21300739+1210330	1.07	1.22	2.68	0.71	4437	4320	4425	4360	4386	13.252	−0.49	2.19
21300569+1210156	0.81	0.98	2.34	0.66	4777	4776	4723	4499	4694	13.472	−0.33	2.01
21300553+1208553	0.88	1.07	2.92	0.80	4680	4588	4249	4136	4413	14.012	−0.52	2.40
21295756+1209438	1.25	1.28	2.86	0.73	4230	4227	4291	4307	4264	11.556	−0.58	2.27
21295082+1211301	0.99	1.09	2.59	0.69	4536	4549	4498	4414	4499	12.778	−0.43	2.15
21295716+1209175	0.83	1.03	2.56	0.73	4749	4669	4523	4307	4562	12.303	−0.42	2.14
					M2							
21333827−0054569	0.93	1.04	2.83	0.79	4640	4639	4312	4157	4437	11.990	−0.54	2.28
21333095−0052154	1.00	1.05	2.65	0.69	4540	4618	4447	4412	4504	13.025	−0.47	2.18
21332468−0044252	1.00	1.07	2.55	0.62	4540	4579	4530	4617	4566	14.030	−0.43	2.11
21331771−0047273	1.23	1.26	2.95	0.75	4251	4250	4230	4254	4246	12.190	−0.64	2.30
21331723−0048171	1.34	1.35	3.18	0.83	4110	4122	4090	4066	4097	12.721	−0.75	2.42
21331790−0048198	1.07	1.10	3.68	1.07		4521	*3912*	3618	4017	13.584	−0.97	2.71
21331854−0051563	0.93	1.07	2.67	0.71	4640	4579	4431	4358	4502	13.231	−0.47	2.19
21331948−0051034	0.93	1.09	2.79	0.81	4640	4540	4340	4111	4408	13.428	−0.51	2.28
21331923−0049058	1.22	1.20	3.59	1.03		4345	*3950*	3682	3992	14.083	−0.94	2.64
21332588−0046004	0.92	1.01	2.69	0.78	4655	4701	4416	4181	4488	13.814	−0.44	2.25
21333668−0051058	1.17	1.21	3.04	0.81	4314	4328	4173	4111	4232	12.271	−0.66	2.37
21333520−0046089	1.16	1.22	2.97	0.76	4326	4312	4217	4229	4271	12.528	−0.65	2.32
21333488−0047572	1.25	1.27	3.09	0.88	4215	4235	4143	3959	4138	12.813	−0.67	2.41
21333593−0049224	1.32	1.35	3.17	0.86	4133	4122	4096	4001	4088	13.002	−0.74	2.42
21333432−0051285	1.11	1.17	2.79	0.70	4391	4395	4340	4384	4378	12.980	−0.55	2.23
21332531−0052511	1.09	1.11	2.77	0.77	4417	4502	4355	4205	4370	13.414	−0.51	2.26
21333109−0054522	1.35	1.39	3.04	0.75	4098	4070	4173	4254	4149	13.675	−0.71	2.33
21333507−0051097	1.10	1.16	2.60	0.58	4404	4412	4488	4746	4512	14.102	−0.49	2.10
					M71							
19535325+1846471	1.39	1.54	3.75	0.86		3908	*3881*	3999	3929	10.455	−1.14	2.61
19534750+1846169	1.11	1.12	2.85	0.71	4466	4496	4307	4355	4406	11.760	−0.57	2.28
19535150+1848059	1.41	1.54	3.61	0.95		3908	*3938*	3821	3889	10.522	−1.02	2.59
19535064+1849075	1.18	1.20	3.08	0.89	4361	4356	4160	3937	4204	11.577	−0.67	2.42
19534575+1847547	1.47	1.65	3.77	0.97			*3873*	3784	3828	10.554	−1.15	2.62
19534827+1848021	1.42	1.49	3.58	1.02		3961	*3951*	3697	3870	10.606	−0.98	2.60
19534656+1847441	0.96	1.02	2.47	0.62	4710	4694	4600	4614	4654	12.438	−0.42	2.06
19535369+1846039	0.70	0.74	2.00	0.58	5289	5410	5096	4742	5134	13.556	−0.21	1.79
19534905+1846003	1.02	1.04	2.61	0.63	4609	4653	4486	4583	4583	12.209	−0.47	2.15
19534916+1846512	0.96	0.95	2.66	0.76	4710	4849	4447	4227	4558	12.434	−0.44	2.22
19534178+1848384	0.96	0.98	2.46	0.71	4710	4781	4610	4355	4614	13.405	−0.37	2.09
19535676+1845399	0.90	0.92	2.38	0.66	4815	4920	4688	4494	4729	13.379	−0.35	2.04
19533962+1848569	0.78	0.80	2.27	0.63	5082	5234	4800	4583	4925	13.636	−0.29	1.98
19533864+1847554	1.03	0.98	2.32	0.50	4593	4781	4748	5029	4788	12.980	−0.34	1.98
19534615+1847261	1.21	1.26	3.08	0.78	4318	4260	4160	4178	4229	11.728	−0.71	2.38
19534941+1844269	1.60	2.20	4.37	0.87			*3676*	3978	3827	9.541	−1.70	2.67

Downloaded from https://academic.oup.com/mnras/article/403/3/1592/1050826 by INAF –IASF Bologna user on 17 January 2023

Table 12. Inferred temperatures, bolometric magnitude and bolometric corrections for target stars in open clusters NGC 188 and NGC 6791.

ID	$(B-V)_o$	$(V-I_C)_o$	$(V-K)_o$	$(J-K)_o$	T_{BV} (K)	T_{VI} (K)	T_{VK} (K)	T_{JK} (K)	$\langle T\rangle$ (K)	Bol_o	BC_V	BC_K
NGC 188												
00445253+851405	1.22	1.20	2.66	0.55	4398	4354	4470	4854	4519	11.552	−0.53	2.13
00475922+851132	1.46	1.27	2.65	0.49	4040	4243	4478	5078	4460	11.311	−0.56	2.09
00465966+851315	1.38	1.16	2.50	0.54	4153	4422	4602	4889	4516	11.701	−0.44	2.06
00554526+851220	1.34	1.35	3.05	0.73	4211	4129	4201	4309	4212	9.842	−0.72	2.33
00463920+852333	1.24	1.22	2.83	0.65	4366	4321	4344	4530	4390	10.706	−0.60	2.23
00472975+852414	1.05	1.04	2.70	0.68	4695	4650	4439	4444	4557	12.166	−0.49	2.21
00441241+850931	1.44	1.47	3.27	0.78	4068	3981	4078	4184	4078	10.165	−0.86	2.41
00432696+850917	0.94	0.93	2.32	0.62	4909	4893	4772	4621	4799	12.578	−0.31	2.02
00490560+852607	1.15	1.11	2.45	0.47	4516	4513	4646	5159	4708	11.945	−0.45	2.00
00420323+852049	1.45	1.48	3.32	0.81	4054	3970	4052	4114	4048	8.628	−0.87	2.46
NGC 6791												
19210807+3747494	1.19	1.09	2.79	0.73	4554	4544	4397	4304	4450	13.100	−0.52	2.27
19205259+3744281	1.47	1.59	3.58	0.91		3844	*3953*	3898	3898	12.720	−1.02	2.56
19205580+3742307	1.21	1.12	2.62	0.59	4518	4488	4527	4712	4561	14.053	−0.48	2.13
19205671+3743074	1.21	1.14	2.66	0.60	4518	4451	4495	4679	4536	13.773	−0.50	2.15
19210112+3742134	1.34	1.37	3.20	0.80	4294	4098	4138	4133	4166	13.322	−0.80	2.40
19211606+3746462	1.43	3.10	5.58	1.01			*3418*	3715	3566	10.646	−2.73	2.85
19213656+3740376	1.39	1.42	3.25	0.84	4214	4035	4111	4043	4101	12.902	−0.81	2.44
19210326+3741190	1.21	1.19	2.71	0.61	4518	4365	4456	4647	4496	13.493	−0.53	2.17
19213635+3739445	1.22	1.08	2.86	0.83	4499	4563	4348	4065	4369	13.867	−0.53	2.33
19212437+3735402	1.25	1.12	2.84	0.78	4446	4488	4361	4180	4369	13.561	−0.54	2.30
19212674+3735186	1.23	1.23	2.87	0.73	4482	4299	4341	4279	4350	13.034	−0.58	2.29
19211632+3752154	1.12	1.12	2.73	0.72	4686	4488	4441	4330	4486	13.119	−0.50	2.23
19211176+3752459	1.15	1.08	2.65	0.66	4629	4563	4503	4496	4548	13.538	−0.48	2.17
19202345+3754578	1.65	2.98	5.64	1.06			*3407*	3633	3520	9.718	−2.72	2.92
19205149+3739334	1.48	2.72	5.11	1.06			*3504*	3633	3568	9.043	−2.25	2.85
19203285+3753488	1.46	3.20	5.88	1.21			*3368*	3416	3392	10.107	−2.92	2.96
19200641+3744452	1.21	1.26	3.15	0.86	4518	4253	4166	4000	4234	12.259	−0.72	2.43
19200882+3744317	1.43	3.76	6.58	1.14			*3260*	3512	3386	9.664	−3.59	2.99
19203219+3744208	1.33	4.35	7.52	1.19			*3120*	3443	3282	9.934	−4.47	3.05

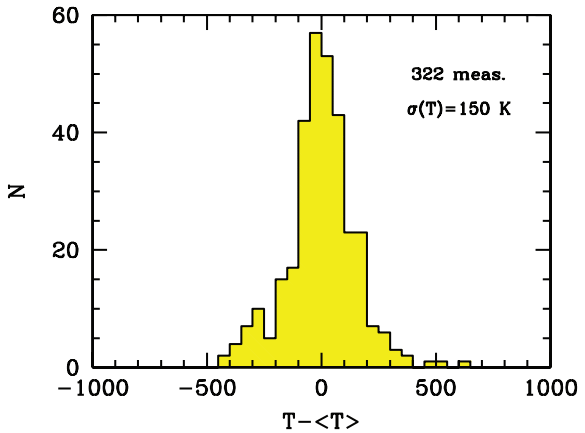

Figure 6. Histogram of temperature difference for all the data reported in Tables 8 and 9 (columns 6–9) with respect to the adopted mean estimate ($\langle T\rangle$ of column 10). A total of 322 entries are available for the whole stellar sample. The resulting distribution gives a direct measure of the internal uncertainty of our temperature scale, amounting to $\sigma(T_{\rm eff}) = \pm 150$ K for the standard individual estimate.

metal-poor ([Fe/H] < -1.0 dex, dots) and metal-rich ([Fe/H] > -1.0 dex, triangles) objects differently. For better convenience in our study, we also fitted the overall distribution analytically; a useful set of fitting functions for the BC versus $T_{\rm eff}$ relations along the $3300 \lesssim T_{\rm eff} \lesssim 5000$ K temperature range results in the following:

$$\begin{cases} BC_V = -\exp(27\,500/T_{\rm eff})/1000 \\ \qquad\qquad (\sigma_{\rm BC}, \rho) = (0.11, 0.989), \\ BC_K = -6.75\log(T_{\rm eff}/9500) \\ \qquad\qquad (\sigma_{\rm BC}, \rho) = (0.05, 0.978). \end{cases} \quad (4)$$

As for the colour relations, the non-monotonic trend of BC_V versus $(B-V)$ (see upper left-hand panel in Fig. 8) prevents us to use the colour as an independent (i.e. 'input') variable in our fit. In this case we had therefore to adjust an inverse relation, assuming BC as the running variable. The corresponding set of analytical solutions, along the same temperature range as that in the previous equation set, eventually results in the following:

$$\begin{cases} B-V = 1.906\,\left[BC_V^2\exp(BC_V)\right]^{0.3} \\ \qquad\qquad (\sigma_{BV}, \rho) = (0.11, 0.863), \\ V-K = 1/(1-0.283\,BC_K) \\ \qquad\qquad (\sigma_{VK}, \rho) = (0.13, 0.991). \end{cases} \quad (5)$$

All these fits are superposed to the data of Fig. 8 as a solid line.

Just on the basis of our data note how difficult it is to firmly constrain the $(B-V)$ versus BC_V behaviour at very low temperature. On one hand, in fact, the intervening effect of the TiO absorption at visual wavelength (Kučinskas et al. 2005) makes the $(B-V)$

Downloaded from https://academic.oup.com/mnras/article/403/3/1592/1050826 by INAF –IASF Bologna user on 17 January 2023

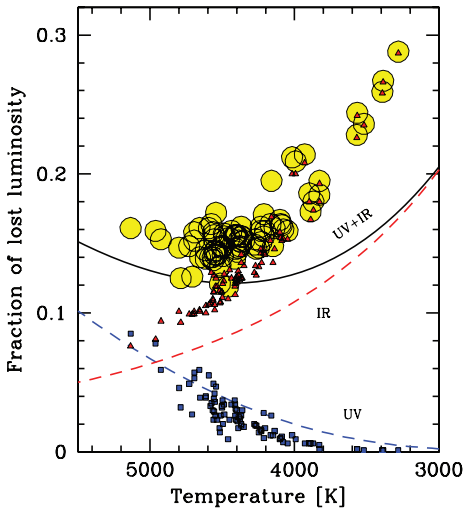

Figure 7. Estimated fraction of unsampled stellar luminosity for the stars in our sample (big solid dots). The relative contribution to stellar bolometric luminosity from lost emission at short (i.e. for $\lambda \leq 4000$ Å, small square markers on the plot) and long (i.e. for $\lambda \geq 2.25$ μm, small triangles) wavelength is sized up by extrapolating the observed SED with two blackbody (BB) 'wings' at fixed $\langle T \rangle$, as from column 10 of both Tables 11 and 12. The same exercise is carried out for a full BB spectrum along the 5500–3000 K temperature range (dashed lines labelled 'UV' and 'IR' for the short and long wavelength contribution, respectively, together with their summed contribution, as in the solid line). Compared to a plain BB case, note that real stars at cool temperatures display a brighter IR luminosity.

colour of stars that are cooler than ∼3700 K saturate strongly, reaching a maximum of about $(B-V)_{\rm max} \simeq 1.5$ and turning back to bluer values for later M-type stars. On the other hand, the apparent trend in our sample in this range is evidently biased by the NGC 6791 stellar population with just a few super-metal-rich giants constraining the BC_V trend at the most extreme negative values.

5.2 BC response to metallicity

As a part of our observing strategy, the sampled stellar population of the five clusters would in principle allow one to better single out any possible dependence of BC on stellar chemical composition. As far as helium content is concerned, for instance, this problem has already been tackled by Girardi et al. (2007) through a series of theoretical models based on the Kurucz (1992) ATLAS9 model atmospheres. As a main result of their discussion, these authors did not find any relevant impact on stellar BC to optical photometric bands when helium changes up to $\Delta Y = +0.2$, *for fixed effective temperature*. To some extent, this is a not-so-surprising behaviour; helium is in fact a substantial contributor to mean particle weight of stellar plasma but a negligible contributor to chemical opacity. Accordingly, with varying Y in the chemical mix, one has to expect a much more explicit impact on stellar temperature *for fixed mass of stars*, rather than on colours or SED *for fixed effective temperature* (as explored by Girardi et al. 2007 models, indeed).

The situation might in principle be different for the metals, mainly through their pervasive effect on stellar blanketing at short wavelength. In addition, metals are the basic ingredients required to

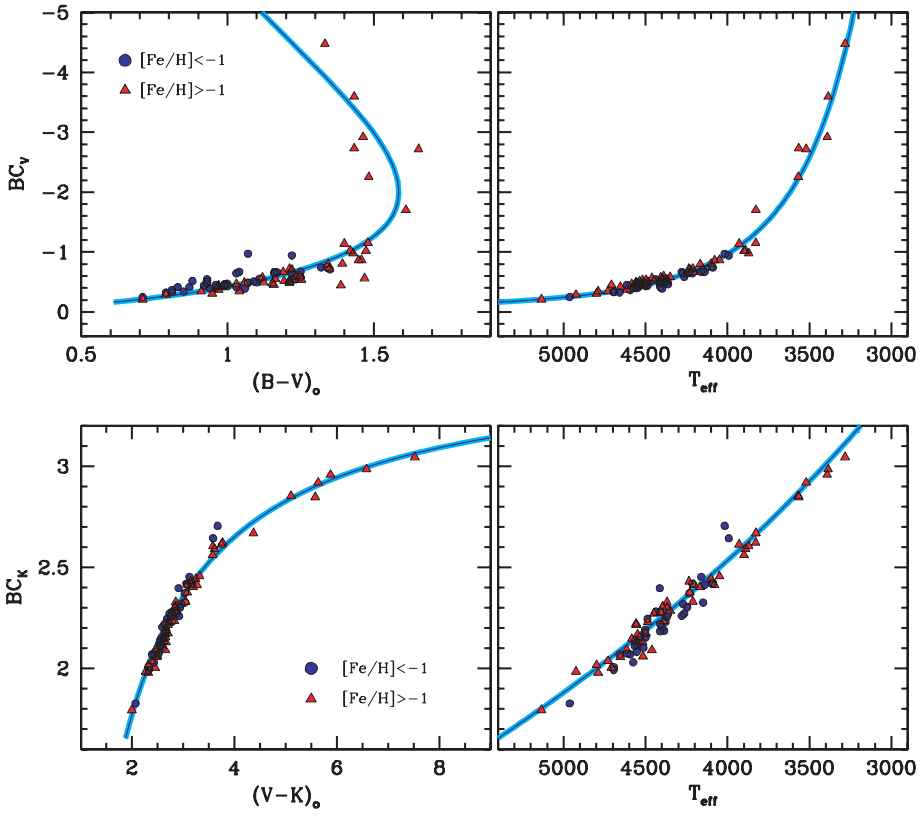

Figure 8. The BC versus colour (left-hand panels) and BC versus $T_{\rm eff}$ (right-hand panels) distribution of our stellar sample (dots and triangles, for metal-poor and metal-rich stars, respectively). Synthetic colours have been corrected for Galactic reddening. Solid lines are our derived calibrations, according to the set of equations (4) and (5).

Downloaded from https://academic.oup.com/mnras/article/403/3/1592/1050826 by INAF –IASF Bologna user on 17 January 2023

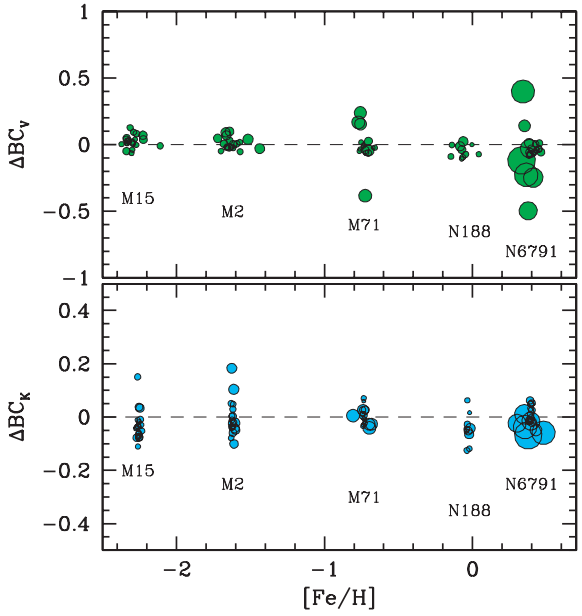

Figure 9. The distribution of BC residuals for our stellar sample versus cluster metallicity. The displayed ΔBC is intended as the difference between the values of columns 12 and 13 of both Tables 11 and 12 and the output of equation (4) entering along with the adopted effective temperature of stars, as in column 10 of the tables. Note the lack of any evident correlation with [Fe/H], as discussed in more detail in Section 5.2. Data in the plot have been slightly spread around the cluster [Fe/H] value for better reading. Dot size is inversely proportional to star temperature (i.e. bigger dots = cooler red giants).

produce molecules like TiO, SiH or CH, whose impact may be extremely relevant at blue and visual wavelength, when effective temperature lowers below 3500 K (Kučinskas et al. 2005; Bertone et al. 2008).

Taking the results of Tables 11 and 12 as a reference, in Fig. 9 we plot the BC residual distribution computed as a difference between the inferred BC (columns 12 and 13 in the tables) and the 'mean' locus of equation (4), once entering the equations with the fiducial $\langle T \rangle$ of column 10. The BC residuals are displayed along the [Fe/H] distribution of the five star clusters, as labelled on the plots. Just a glance to both panels of the figure makes evident the lack of any drift of BC with stellar metallicity. Within the accuracy limits of our analysis, this means that two red giant stars of the same effective temperature but different [Fe/H] have virtually indistinguishable values of BC to V and K bands.

On the other hand, to correctly understand our conclusion, one has to pay attention to the different temperature regimes that mark spectral properties of red giant stars. In fact, stars warmer than ∼4000 K may have their SED depressed at short wavelength mostly in force of *atomic* transitions of Fe and other metals; on the contrary, for a cooler temperature, the metal opacity mainly acts in the form of *molecular* absorptions, making the broad-band systems the prevailing features that modulate the stellar SED. As a consequence, while for stars of spectral type G or earlier any change of Z simply implies a change in the blanketing strength, this may not straightforwardly be the case for later spectral types, where molecules play a much more entangled role with changing $T_{\rm eff}$.

In order to better quantify the terms of our analysis, in this respect, we display in Fig. 10 the temperature distribution of stars in our sample across the metallicity range spanned by the five clusters considered. As a striking feature, note that only for NGC 6791 we

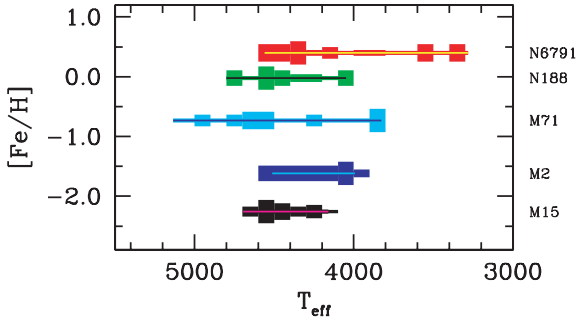

Figure 10. Temperature distribution of red giant stars in each of the five clusters of our sample, according to Tables 11 and 12. Line thickness is proportional to the star density along the spanned temperature range. Note that only cluster NGC 6791 contains stars cooler than ∼3800 K.

are able to probe stars cooler than ∼3800 K. The obvious *caveat* in our discussion is therefore that we can only assess the impact of *atomic* blanketing on stellar BC, while no firm conclusions can be drawn for the BC dependence on molecular absorption, facing the evident bias of our star sample against cool ($T_{\rm eff} \ll 4000$) objects.

As far as the blanketing is the prevailing mechanism at work in G–K stars, the basic physics of stellar atmospheres leads one to conclude that the V-band (and even more the K-band) luminosity is nearly unaffected by metal absorption, so that BC cannot vary much with [Fe/H]. Rather, B (and even more U) magnitudes must be more strongly modulated by metal abundance making BC_B (and BC_U) more directly sensitive to [Fe/H]. On the other hand, as $\mathrm{BC}_B = \mathrm{BC}_V - (B - V)$, one can straightaway 'translate' this metallicity effect in terms of apparent $(B - V)$ colour change. This is shown in Fig. 11, where, for each star in our sample, we have computed the residual $(B - V)$ and $(V - K)$ colour as a difference between observed and expected values by entering in equation (5) the fitted value of BC as from equation (4). Metallicity is traced

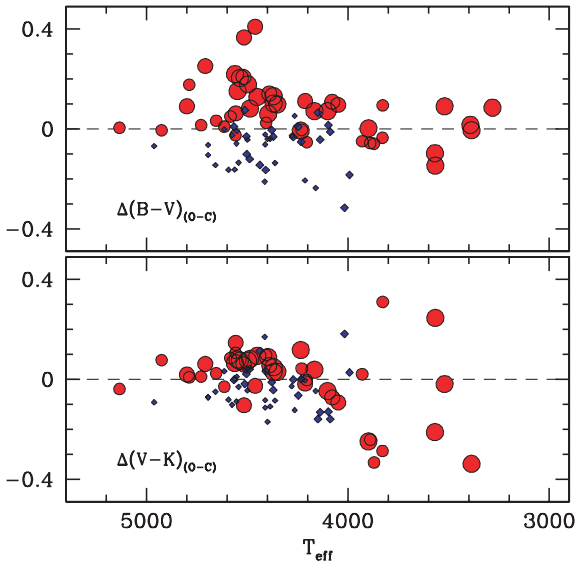

Figure 11. Residual $(B - V)$ and $(V - K)$ distribution versus stellar temperature for stars in Tables 11 and 12. Colour residual is computed as a difference between observed and expected values by entering equation (5) along with the BC output of equation (4). Metal-poor and metal-rich stars are singled out by diamonds and dot markers, respectively, taking the value [Fe/H] = −1.0 dex as a reference threshold. Marker size increases with [Fe/H], throughout.

Downloaded from https://academic.oup.com/mnras/article/403/3/1592/1050826 by INAF –IASF Bologna user on 17 January 2023

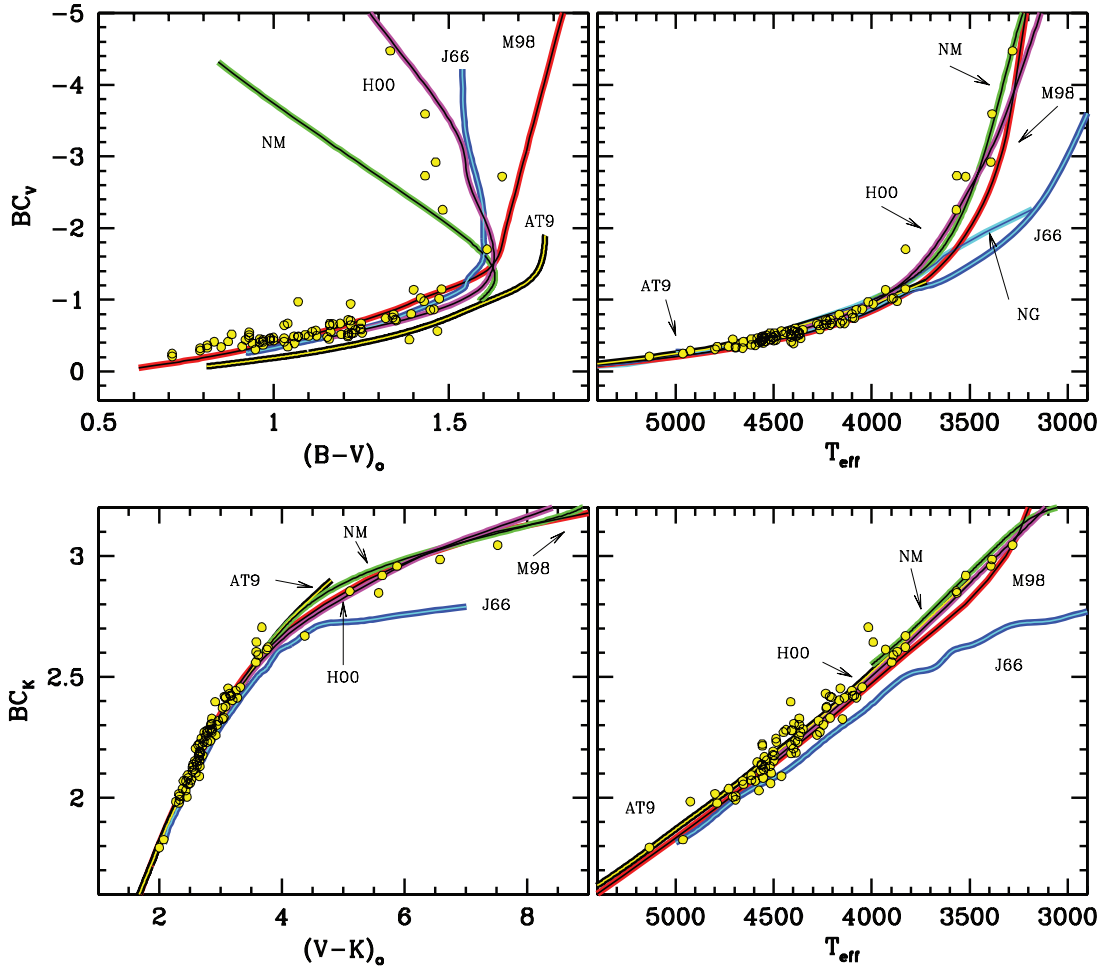

Figure 12. Same as Fig. 8, but comparing our data with different theoretical and empirical calibrations from Johnson (1966, 'J66' labels), Bertone et al. (2004) using ATLAS9 (Kurucz 1992, 'AT9') and NEXTGEN (Hauschildt et al. 1999, 'NG') synthesis codes for model atmosphere computation, Montegriffo et al. (1998, 'M98') and Houdashelt et al. (2000, 'H00') using MARCS theoretical code by Bell & Gustafsson (1978), and its updated version (NMARCS), as in Plez et al. (1992) and Bessell et al. (1998, 'NM').

in the plot by the marker size (the bigger the marker the higher the [Fe/H] value); again, we discriminate between metal-poor (diamonds) and metal-rich (dots) stars, taking the value [Fe/H] $= -1.0$ dex as a reference threshold.

A trend of $\Delta(B-V)$ versus cluster metallicity is now clearly evident, with the metal-poor and metal-rich star samples neatly segregated in the plot, the latter stars displaying a 'redder' $(B-V)$ colour (and correspondingly a positive colour residual) *for fixed effective temperature*. On the contrary, note that both 'metal-poor' and 'metal-rich' stars are well mixed in the $\Delta(V-K)$ plot, witnessing once more the property of the $V-K$ colour as a virtually metal-independent feature.

Considering in more detail the $\Delta(B-V)$ distribution versus cluster metallicity, a fit to the data provides the following:[8]

$$-\Delta\mathrm{BC}_B \equiv \Delta(B-V) = \underset{\pm 1}{0.10}\ [\mathrm{Fe/H}] + \underset{\pm 2}{0.13} \qquad (6)$$

with error bars at 1σ level and (rms, ρ) = (0.09 mag, 0.70).

[8]Of course, following our previous arguments, we had to exclude from our analysis cluster NGC 6791, for its obvious bias in constraining the empirical $T_{\rm eff}$ versus $(B-V)$ relationship for stars at supersolar metallicity.

5.3 Comparison with other BC scales

For a better understanding of our results, it is relevant to compare our output with other popular calibration scales often taken as a reference in the current literature and especially to attempt to extend their analysis to cool ($T_{\rm eff} \lesssim 3500$ K) stellar temperatures. In particular, we will focus here on different theoretical BC calibrations relying on the three leading codes for advanced computation of stellar model atmospheres, namely ATLAS9 (Kurucz 1992, hereafter labelled as 'AT9'), NEXTGEN (Hauschildt, Allard & Baron 1999, 'NG'), both as reported by Bertone et al. (2004), and MARCS (Bell & Gustafsson 1978, as adopted by Houdashelt et al. 2000, 'H00' label) also in its updated versions (NMARCS, as in Plez, Brett & Nordlund 1992; Bessell et al. 1998, 'NM').

We will also consider in our analysis two empirical studies, i.e. the ones of Johnson (1966, referred to as 'J66') and Montegriffo et al. (1998, labelled as 'M98'), both based on a careful analysis of infrared colours to assess the problem of the bolometric correction and a self-consistent temperature scale for red giant stars. All the bolometric scales in the figure have been shifted such as to agree with our assumption that $\mathrm{BC}_V^{\odot} = -0.07$ mag.

A synoptic look of the different theoretical and empirical frameworks is eased by the four panels of Fig. 12, where we report the

Downloaded from https://academic.oup.com/mnras/article/403/3/1592/1050826 by INAF –IASF Bologna user on 17 January 2023

BC_V and BC_K scales versus observables [i.e. $(B-V)$ and $(V-K)$ colours, respectively] and theoretical ($T_{\rm eff}$) reference quantities. In all respects, this figure is fully equivalent to, and can be compared to, Fig. 8, where we have reported our own results.

Just a quick look to the different curves of Fig. 12 gives an immediate picture of the inherent uncertainties in predicted BC according to the different calibration scales. The big issue, in this regard, much deals with the way models can reproduce cool stars and observations can account for the $(B-V)$ 'saturation' versus temperature consequent to the shifted emission towards longer wavebands when stars become cooler than 3500 K. This effect makes the *B*-luminosity contribution to drop to nominal values among red giants, and the increasingly important role of molecular absorption strongly modulates optical colours of K- and M-type stars.

The still inadequate theoretical performance in modelling such cool stars with convenient accuracy fatally frustrates also any empirical effort to derive a firm temperature scale and an accurate abundance analysis for stars at the extreme edge of the temperature distribution (see e.g. Bertone et al. 2008 and Olling et al. 2009, for useful considerations on this subject).

As far as the BC_V versus $(B-V)$ behaviour is concerned, the reference calibrations display the largest spread, with M98 predicting increasingly redder stars with decreasing temperature. On the opposite, NM predicts a sharp colour 'turnback', with BC_V increasing in absolute value among cool stars getting bluer and bluer. Definitely, the empirical calibration by J66 still remains a reference one, tracking the observations fairly well. This trend is also replied very closely by the MARCS models by H00, that provide an even better match to the data and a substantial agreement with our fitting function as in Fig. 8.

On conversion of colours to the theoretical plane of effective temperature (upper right-hand panel of Fig. 12), the picture slightly changes, in particular with a striking discrepancy of the J66 and the theoretical NG temperature scale for $T_{\rm eff} \lesssim 3800$ K. Both sources predict, in fact, much shallower corrections for cool stars than we observe. An overall agreement has to be reported, on the contrary, among the other calibrations, all replying our equation (4).

The situation is much eased in the infrared domain, where a monotonic relationship between $(V-K)$ colour and BC_K characterizes red giants stars. In this new framework, both the theoretical and empirical planes are well reproduced by the different calibration scales, with the only remarkable exception of J66 that, to some extent 'allows' stars to store a bigger fraction of their bolometric luminosity in the infrared. This leads to a tipping $BC_K \simeq 2.7$ and a too 'red' $(V-K)$ for a given value of $T_{\rm eff}$.

Combining the different pieces of information coming from these comparisons, it seems that the H00 MARCS models are by far the best ones in matching our BC estimates, closely replying in every panel of Fig. 12 our empirical fitting functions of equations (4) and (5) and Fig. 8. In spite of this comforting appearance, however, this conclusion may be even more puzzling from a physical point of view, as the H00 models have been a fortiori tuned up such as to reproduce the observed colours of M stars. As described by the authors, this is required in particular to strongly enhance the assumed TiO opacities well beyond the admitted physical range suggested by molecular theory and implemented in the 'standard' MARCS library (Gustafsson et al. 2008).

6 SUMMARY AND CONCLUSIONS

A firm knowledge of a fully reliable link between observations and stellar evolution models is a basic, crucial requirement for any safe use of stellar clocks and population synthesis templates in the study and interpretation of the integrated spectrophotometric properties of distant galaxies. Actually, the 'stellar path' to cosmology is strictly dependent, among others, on the accurate determination of the bolometric emission of stars, with varying effective temperatures and chemical abundance.

In this framework, we have tackled the central question of the possible BC dependence on stellar metallicity by securing spectroscopic observations for a wide sample of 92 red giant stars in five (three globular + two open) Galactic clusters along the full metallicity range from [Fe/H] $= -2.2$ up to $+0.4$ (see Section 3). The spectra cover the wavelength range from 3500 Å to 2.5 μm, collecting optical and IR observations. As a delicate task for the final settlement of our stellar data base, we dealt with the accurate flux calibration and a consistent match of the optical and near-IR sides of the spectra such as to reproduce, for each star, the broad-band $BVR_{\rm C}\ I_{\rm C}\ JHK$ photometry available in the literature (Sections 2 and 3). Overall, we are confident that stellar SED along the entire sampled wavelength range was set up within a ± 10 per cent internal accuracy (see Table 7 and Fig. 3).

According to our previous arguments, however, one has also to carefully account for the lost contribution of ultraviolet and far-IR luminosity to the bolometric flux, depending on the effective temperature of stars. Based on the Alonso et al. (1999) $T_{\rm eff}$–colour fitting functions, we took the four colours $(B-V)$, $(J-K)$, $(V-I_{\rm C})$ and $(V-K)$ as a reference for our calibration, leading to the constraining of $T_{\rm eff}$ for each stars in our sample within an estimated error better than ± 100 K (see Section 4.1), along the whole spanned temperature range ($3300 \leq T_{\rm eff} \leq 5000$ K).

The fiducial temperature allowed us to shape the unsampled portion of the SED at UV and far-IR wavelength by assuming a blackbody emission independently rescaled such as to connect the short- and long-wavelength edge of the observed spectra. As shown in Section 4.2 (see also Fig. 7), under the blackbody assumption, the internal uncertainty in our temperature scale only impact by a few 0.01 mag uncertainty in the inferred bolometric magnitude of our stars. In any case, by fully neglecting any unsampled spectral contribution, our data would be overestimating $M_{\rm bol}$ by at most 0.3 mag.

Making use of our new data base, we have been able to draw a convenient set of fitting functions for the BC versus $T_{\rm eff}$, valid over the interval $3300 \leq T_{\rm eff} \leq 5000$ K (see Section 5.1, equation 4). Similar relationships for BC versus stellar colours cannot be straightforwardly derived (equation 5), especially for the $(B-V)$, which shows a strong saturation effect for stars cooler than 3700 K, in consequence of the intervening TiO absorption at visual wavelength (Kučinskas et al. 2005). In assessing properties of such very cool stars, however, one has also to consider that our sample is strongly biased against high-metallicity values as only the red giant branch of NGC 6791 ([Fe/H] $= +0.4$) hosts stars with $T_{\rm eff} <$ 3700 K.

Thanks to the wide [Fe/H] range spanned by G stars in the five clusters considered here, we explored the possible BC dependence on stellar metallicity. As far as atomic transitions prevail as the main source of metal opacity in the spectra of relatively warm ($T_{\rm eff} \gtrsim$ 4000 K) stars, our data confirm that no evident trend of BC with [Fe/H] is in place (see Fig. 9). In other words, two red giant stars of the same effective temperature but different [Fe/H] are virtually indistinguishable in the values of BC to *V* and *K* bands. Things may be different, however, for the *B* (and even more for *U*) magnitudes, where the blanketing effects are more and more severe. In fact, Fig. 11 clearly shows that metal-poor stars display a 'bluer' $(B-V)$ compared to corresponding metal-rich objects with the same

Downloaded from https://academic.oup.com/mnras/article/403/3/1592/1050826 by INAF –IASF Bologna user on 17 January 2023

$T_{\rm eff}$. This leads us to conclude that a drift may be expected for BC_B such as $BC_B \propto -0.10\,[Fe/H]$ among stars with fixed value of $T_{\rm eff}$.

To consistently verify our calibrations, we have shown in Fig. 12 plots of BC_V and BC_K versus colours and $T_{\rm eff}$, respectively, by comparing with different theoretical and empirical calibrations currently available in the literature. As far as theoretical predictions are concerned, it seems that the H00 models are the best ones matching our data in every relationship. This feature is not a surprising one, however, given the recognized intention of the H00 calculations to match M stars via ad hoc tuning of molecular opacity. Actually, this successful comparison may add a further piece of evidence, all the way, to the persisting limitation of theory to independently assess the modelling of cool stars.

ACKNOWLEDGMENTS

We thank Paolo Montegriffo and Livia Origlia for useful advises and contributions to the discussion of our results. An anonymous referee is also acknowledged for a very careful review of the paper, and for illuminating suggestions about the main focus of the paper.

With pleasure we also acknowledge partial financial support of the Italian INAF through grant PRIN07-1.06.10.04 and the Fundación G. Galilei of La Palma. This work made use of the SIMBAD data base, operated by CDS, Strasbourg, France, and of the data products from the Two Micron All Sky Survey, which is a joint project of UMASS and the CALTECH Infrared Processing and Analysis Center, USA, funded by NASA and NSF.

REFERENCES

Alonso A., Arribas S., Martínez-Roger C., 1999, A&AS, 140, 261
Baade W., 1928, Astron. Nachrichten, 232, 65
Bell R. A., Gustafsson B., 1978, A&AS, 34, 229
Bertone E., Buzzoni A., Chávez M., Rodríguez-Merino L. H., 2004, AJ, 128, 829
Bertone E., Buzzoni A., Chávez M., Rodríguez-Merino L. H., 2008, A&A, 485, 823
Bessell M. S., 1979, PASP, 91, 589
Bessell M. S., Wood P. R., 1984, PASP, 96, 247
Bessell M. S., Castelli F., Plez B., 1998, A&A, 333, 231
Blackwell D. E., Lynas-Gray A. E., 1994, A&A, 282, 899
Blackwell D. E., Shallis M. J., Selby M. J., 1979, MNRAS, 188, 847
Blackwell D. E., Petford A. D., Shallis M. J., 1980, A&A, 82, 249
Buzzoni A., 1989, ApJS, 71, 817
Buzzoni A., 2005, MNRAS, 361, 725
Cassisi S., Salaris M., Castelli F., Pietrinferni A., 2004, ApJ, 616, 498
Code A. D., Bless R. C., Davis J., Brown R. H., 1976, ApJ, 203, 417
Cohen J. G., Briley M. M., Stetson P. B., 2005, AJ, 130, 1177
de Marchi F. et al., 2007, A&A, 471, 515
di Benedetto G. P., Rabbia Y., 1987, A&A, 188, 114
Dyck H. M., Benson J. A., van Belle G. T., Ridgway S. T., 1996, AJ, 111, 1705
Flower P. J., 1975, A&A, 41, 391
Flower P. J., 1977, A&A, 54, 31
Flower P. J., 1996, ApJ, 469, 355
Frogel J. A., Persson S. E., Matthews K., Aaronson M., 1978, ApJ, 220, 75
Fuensalida J. J., Alonso A., 1998, New Astron. Rev., 42, 543
Geffert M., Maintz G., 2000, A&AS, 144, 227
Girardi L., Castelli F., Bertelli G., Nasi E., 2007, A&A, 468, 657
González Hernández J. I., Bonifacio P., 2009, A&A, 497, 497
Gratton L., Gaudenzi S., Rossi C., Gratton R. G., 1982, MNRAS, 201, 807
Gustafsson B., Edvardsson B., Eriksson K., Jørgensen U. G., Nordlund Å., Plez B., 2008, A&A, 486, 951
Hauschildt P. H., Allard F., Baron E., 1999, ApJ, 512, 377
Houdashelt M. L., Bell R. A., Sweigart A. V., 2000, AJ, 119, 1448
Hunt L. K., Mannucci F., Testi L., Migliorini S., Stanga R. M., Baffa C., Lisi F., Vanzi L., 1998, AJ, 115, 2594
Johnson H. L., 1966, ARA&A, 4, 193
Kaluzny J., Rucinski S. M., 1995, A&AS, 114, 1
Kučinskas A., Hauschildt P. H., Ludwig H.-G., Brott I., Vansevičius V., Lindegren L., Tanabé T., Allard F., 2005, A&A, 442, 281
Kuiper G. P., 1938, ApJ, 88, 429
Kurucz R. L., 1992, in Barbuy B., Renzini A., eds, Proc. IAU Symp. 149, The Stellar Populations of Galaxies. Kluwer, Dordrecht, p. 225
Lançon A., Mouhcine M., 2002, A&A, 393, 167
Lang K. R., 1991, Astrophysical Data: Planets and Stars. Springer-Verlag, Heidelberg
Manduca A., Bell R. A., 1979, PASP, 91, 848
Massey P., Strobel K., Barnes J. V., Anderson E., 1988, ApJ, 328, 315
Mochejska B. J., Stanek K. Z., Kaluzny J., 2003, AJ, 125, 3175
Montegriffo P., Ferraro F. R., Origlia L., Fusi Pecci F., 1998, MNRAS, 297, 872
Olling R. P. et al., 2009, Astro2010: The Astronomy and Astrophysics Decadal Survey, Science White Papers, no., 226 (astro-ph/0902.3197)
Perrin G., Coude Du Foresto V., Ridgway S. T., Mariotti J.-M., Traub W. A., Carleton N. P., Lacasse M. G., 1998, A&A, 331, 619
Platais I., Kozhurina-Platais V., Mathieu R. D., Girard T. M., van Altena W. F., 2003, AJ, 126, 2922
Plez B., Brett J. M., Nordlund A., 1992, A&A, 256, 551
Ramírez I., Meléndez J., 2005, ApJ, 626, 446
Richichi A., Ragland S., Stecklum B., Leinert C., 1998, A&A, 338, 527
Ridgway S. T., Jacoby G. H., Joyce R. R., Wells D. C., 1980, AJ, 85, 1496
Rosenberg A., Piotto G., Saviane I., Aparicio A., 2000, A&AS, 144, 5
Scheffler H., 2006, in Martienssen W., ed., Landolt-Börnstein – Numerical Data and Functional Relationships in Science and Technology – New Series – Group VI Astronomy and Astrophysics, Chap. 7. Springer-Verlag, Heidelberg, p. 46
Skrutskie M. F. et al., 2006, AJ, 131, 1163
Stetson P. B., Bruntt H., Grundahl F., 2003, PASP, 115, 413
Stetson P. B., McClure R. D., VandenBerg D. A., 2004, PASP, 116, 1012
Tokunaga A. T., Vacca W. D., 2005, PASP, 117, 421
Tripicco M. J., Bell R. A., 1995, AJ, 110, 3035
VandenBerg D. A., Clem J. L., 2003, AJ, 126, 778
Wesselink A. J., 1969, MNRAS, 144, 297
Worthey G., Lee H., 2006, ApJS, submitted (astro-ph/0604590)

This paper has been typeset from a TEX/LATEX file prepared by the author.

Downloaded from https://academic.oup.com/mnras/article/403/3/1592/1050826 by INAF –IASF Bologna user on 17 January 2023